

Efficient QR-Based CP Decomposition Acceleration via Dimension Tree and Extrapolation

Wenchao Xie*, Jiawei Xu[†], Zheng Peng[‡], Qingsong Wang[§]

Abstract

The canonical polyadic (CP) decomposition is one of the most widely used tensor decomposition techniques. The conventional CP decomposition algorithm combines alternating least squares (ALS) with the normal equation. However, the normal equation is susceptible to numerical ill-conditioning, which can adversely affect the decomposition results. To mitigate this issue, ALS combined with QR decomposition has been proposed as a more numerically stable alternative. Although this method enhances stability, its iterative process involves tensor-times-matrix (TTM) operations, which typically result in higher computational costs. To reduce this cost, we propose branch reutilization of dimension tree, which increases the reuse of intermediate tensors and reduces the number of TTM operations. This strategy achieves a 33% reduction in computational complexity for third and fourth order tensors. Additionally, we introduce a specialized extrapolation method in CP-ALS-QR algorithm, leveraging the unique structure of the matrix \mathbf{Q}_0 to further enhance convergence. By integrating both techniques, we develop a novel CP decomposition algorithm that significantly improves efficiency. Numerical experiments on five real-world datasets show that our proposed algorithm reduces iteration costs and enhances fitting accuracy compared to the CP-ALS-QR algorithm.

Keywords: CP decomposition, ALS, QR decomposition, Dimension tree, Extrapolation.

1 Introduction

Tensors, also known as multidimensional arrays, have been widely studied due to their ability to extend the concept of matrices and efficiently model multidimensional data. This ability makes them a powerful tool in various applications, including signal processing [11, 28], computer vision [41], recommendation systems [32, 37], image processing [36], knowledge bases [6], and other domains [18, 19]. In these applications, tensor methods primarily rely on tensor decomposition, which helps uncover latent structures or estimate missing values in data. Several tensor decomposition techniques have been developed, each characterized by a distinct way of decomposing tensor components. Common methods include canonical polyadic (CP) decomposition [16, 17], Tucker decomposition [40], tensor train decomposition [29], tensor ring decomposition [43], and block term decomposition (BTD) [33]. Among these, CP decomposition is one of the most fundamental and widely used approaches, see, e.g. [2, 13, 19, 20, 23, 34]. It represents a tensor as a sum of rank-1 components, making it a natural extension of matrix factorization to higher-order data. Due to its strong interpretability and

*School of Mathematics and Computational Science, Xiangtan University, Xiangtan, 411105, China. Email: youmengx@hotmail.com

[†]School of Mathematics and Computational Science, Xiangtan University, Xiangtan, 411105, China. Email: xujiawei@smail.xtu.edu.cn

[‡]School of Mathematics and Computational Science, Xiangtan University, Xiangtan, 411105, China. Email: pzheng@xtu.edu.cn

[§]Corresponding author. School of Mathematics and Computational Science, Xiangtan University, Xiangtan, 411105, China. Email: nothing2wang@hotmail.com

broad applicability, CP decomposition has been extensively studied, leading to various numerical algorithms for its computation. The most commonly used algorithm is the alternating least squares (ALS) [7, 15] method, which iteratively updates factor matrices to minimize reconstruction error [30, 42]. While the ALS algorithm is simple and easy to implement, its convergence speed is relatively slow, which limits its practical efficiency. To address this issue, various improvements to the CP-ALS algorithm have been proposed to enhance both efficiency and convergence. For example, Chen et al. [8] introduced a higher-order search direction and an adaptive step size selection strategy to accelerate the ALS algorithm. Li et al. [21] developed a nonlinear least squares method based on Gauss-Newton optimization to minimize the L_2 norm of the approximation residual, yielding a more effective low-rank CP decomposition. Rajih et al. [31] extended the ALS algorithm by incorporating a more sophisticated extrapolation technique that leverages nonlinear parameter trends and updates all parameter sets simultaneously. In addition to the ALS algorithm, other algorithms have also been developed for solving CP decomposition. Notable examples include those in [9, 26, 38, 39].

As mentioned above, despite some progress in improving the basic ALS framework, challenges remain in tackling complex and large-scale problems, particularly when it comes to convergence speed. To address these challenges, it is crucial to consider the computational difficulties encountered during the optimization process. Specifically, algorithms derived from the ALS framework are required to solve a series of quadratic subproblems, which often involve matrix inversion to obtain the solutions. However, explicit matrix inversion is generally discouraged due to two main drawbacks. First, it incurs a significant computational cost, often scaling at $O(n^3)$ for dense matrices, which becomes prohibitively expensive as the matrix size increases. Second, it is more susceptible to numerical instability, especially when applied to ill-conditioned matrices, thereby compromising the reliability of the solution. To mitigate these issues, researchers have explored alternative strategies to improve the efficiency and stability of ALS-based methods. One effective approach is to replace the conventional normal equation method with QR decomposition when solving quadratic subproblems [24]. Unlike the normal equation method, which requires computing the matrix inverse explicitly, QR decomposition leverages the orthogonality property $\mathbf{Q}^T \mathbf{Q} = \mathbf{I}$ of orthogonal matrices. This not only avoids the numerical instability caused by matrix inversion, but also improves the overall robustness of the algorithm. By integrating QR decomposition into the ALS framework, the solution process becomes more stable and computationally efficient, paving the way for more reliable tensor decomposition methods.

1.1 Motivation and contribution

The CP decomposition employing QR decomposition principles, denoted as CP-ALS-QR [24], solves for the factor matrices by iteratively solving the linear equations of the upper triangular matrix, specifically using the relation $\mathbf{R}\mathbf{X} = \mathbf{Q}^T \mathbf{B}$, where \mathbf{X} represents the factor matrix and \mathbf{B} corresponds to the unfolded tensor. This formulation leverages the triangular structure of \mathbf{R} , transforming the solution process into a sequence of linear equations, which not only greatly reduces the computational burden of matrix inversion but also endows the CP-ALS-QR framework with better numerical stability compared to the CP-ALS framework. However, the CP-ALS-QR algorithm requires multiple tensor-times-matrix (TTM) operations during the iteration process, significantly increasing the computational overhead. This challenge becomes particularly prominent in high-rank scenarios, where its computational complexity markedly exceeds that of the traditional CP-ALS algorithm.

To overcome this limitation, we investigated the use of dimension tree optimization techniques for tensor TTM operations. Although the dimension tree has shown improvements in computational efficiency and complexity both theoretically and experimentally, especially in synthetic tensor scenarios, their performance can fluctuate when applied to real-world tensor datasets. Furthermore, during iterative updates using the dimension tree, some intermediate tensors are underutilized, resulting in inefficient use of the dimension tree. On the other hand, inspired by the widespread use of acceleration techniques, such as Nesterov acceleration [27], momentum acceleration [10], and extrapolation acceleration [3], we apply some acceleration techniques to speed up the CP-ALS-QR algorithm. How-

ever, considering the inherent computational complexity of the algorithm, we mainly explore simpler forms of acceleration to ensure that the computational complexity of the algorithm does not increase significantly, or can even be neglected.

The key contributions of this paper can be summarized as follows.

- We introduce the branch reutilization of dimension tree (BR), which improves the utilization of intermediate tensors in the dimension tree. When integrated with the CP-ALS-QR algorithm, it significantly enhances the iteration efficiency of CP-ALS-QR. Additionally, theoretical analysis in Subsection 3.4 shows that branch reutilization of dimension tree incurs lower computational complexity compared to the dimension tree. For example, it reduces 33% of the computational complexity for third-order and fourth-order tensors.
- We propose an efficient and concise extrapolation method for the matrix \mathbf{Q}_0 within the CP-ALS-QR algorithm. This extrapolation technique leverages the unique structural properties of \mathbf{Q}_0 , where the first element in its first row and first column is 1, and all other elements in the first row and first column are 0. It is specifically designed to accelerate the extrapolation process in the CP-ALS-QR algorithm.
- We propose a new algorithm, ALS-QR-BRE (Algorithm 3), which integrates branch reutilization of dimension tree and extrapolation techniques. Experimental results on both synthetic and real-world tensor datasets demonstrate that ALS-QR-BRE not only accelerates the iteration speed of CP-ALS-QR, but also achieves higher fitting accuracy. In our experiments with real-world tensors, the fitting accuracy is better compared to other compared algorithms.

The organization of this paper is as follows. In Section 2, we introduce the necessary notation and definitions. Section 3 provides the details of the proposed methods, algorithm, and complexity analysis. We present the results of numerical experiments in Section 4. Finally, we conclude the paper in Section 5.

2 Background

In this section, we introduce the essential mathematical notations and fundamental concepts used throughout the paper. We first define the notation for tensors and their basic operations, followed by a discussion of key properties of the CP decomposition. Additionally, we summarize two relevant CP decomposition algorithms: CP-ALS [19] and CP-ALS-QR [24].

2.1 Notation and definitions

The analysis in this paper employs matrix multiplication, tensor algebra, and specialized notation for tensor operations, adhering to the symbolic conventions established in [19]. We denote scalars by lowercase letters (e.g., a), vectors by boldface lowercase letters (e.g., \mathbf{a}), matrices by boldface uppercase letters (e.g., \mathbf{A}), and tensors by calligraphic uppercase letters (e.g., \mathcal{X}).

The Kronecker product of two matrices $\mathbf{A} \in \mathbb{R}^{I \times J}$ and $\mathbf{B} \in \mathbb{R}^{K \times L}$ is denoted by $\mathbf{A} \otimes \mathbf{B} \in \mathbb{R}^{(IK) \times (JL)}$, with the entries given by $[\mathbf{A} \otimes \mathbf{B}]_{(K(i-1)+k, L(j-1)+l)} = \mathbf{A}(i, j)\mathbf{B}(k, l)$. For matrices $\mathbf{A} \in \mathbb{R}^{I \times J}$ and $\mathbf{B} \in \mathbb{R}^{K \times J}$, their Khatri-Rao product results in a matrix of size $(IK) \times J$, defined as $\mathbf{A} \odot \mathbf{B} = [\mathbf{a}_1 \otimes \mathbf{b}_1, \dots, \mathbf{a}_J \otimes \mathbf{b}_J]$. For any matrices $\mathbf{A} \in \mathbb{R}^{J \times I}$, $\mathbf{B} \in \mathbb{R}^{K \times I}$, $\mathbf{C} \in \mathbb{R}^{K \times J}$, and $\mathbf{D} \in \mathbb{R}^{J \times K}$, within the context of Kronecker and Khatri-Rao product operations, the following identity holds:

$$(\mathbf{C} \otimes \mathbf{D})(\mathbf{A} \odot \mathbf{B}) = (\mathbf{CA}) \odot (\mathbf{DB}). \quad (1)$$

The Hadamard product of two matrices $\mathbf{A} \in \mathbb{R}^{I \times J}$ and $\mathbf{B} \in \mathbb{R}^{I \times J}$ is the elementwise product, denoted as $\mathbf{A} * \mathbf{B} \in \mathbb{R}^{I \times J}$, where $[\mathbf{A} * \mathbf{B}](i, j) = \mathbf{A}(i, j)\mathbf{B}(i, j)$. The mode- n product of a tensor $\mathcal{X} \in \mathbb{R}^{I_1 \times \dots \times I_N}$ and a matrix $\mathbf{B} \in \mathbb{R}^{J \times I_n}$ is defined by $\mathcal{Y} = \mathcal{X} \times_n \mathbf{B} \in \mathbb{R}^{I_1 \times \dots \times I_{n-1} \times J \times I_{n+1} \times \dots \times I_N}$, with entries given

by $\mathcal{Y}(i_1, \dots, j, \dots, i_N) = \sum_{i_n=1}^{I_n} \mathcal{X}(i_1, \dots, i_n, \dots, i_N) \mathbf{B}(j, i_n)$. This operation, commonly referred to as TTM (Tensor-Times-Matrix) operation, extends naturally to scenarios where an N -mode tensor is multiplied by multiple matrices along different modes. This extended operation, known as Multi-TTM, is formally defined as:

$$\mathcal{Y} = \mathcal{X} \times_1 \mathbf{B}_1 \times_2 \mathbf{B}_2 \times_3 \cdots \times_N \mathbf{B}_N, \quad (2)$$

where $\mathcal{X} \in \mathbb{R}^{I_1 \times \cdots \times I_N}$, $\mathcal{Y} \in \mathbb{R}^{R_1 \times \cdots \times R_N}$ and $\mathbf{B}_i \in \mathbb{R}^{R_i \times I_i}$. This is expressed in the matricized form as:

$$\mathbf{Y}_{(n)} = \mathbf{X}_{(n)} (\mathbf{B}_N \otimes \cdots \otimes \mathbf{B}_{n-1} \otimes \mathbf{B}_{n+1} \otimes \cdots \otimes \mathbf{B}_1)^T, \quad (3)$$

where $\mathbf{X}_{(n)}$ and $\mathbf{Y}_{(n)}$ represent the mode- n unfolding of tensors \mathcal{X} and \mathcal{Y} , respectively.

2.2 CP decomposition

The CP decomposition [16, 17] is a higher-order extension of matrix singular value decomposition (SVD). It expresses a higher-order tensor as a sum of a finite number of rank-1 tensors. For an N -mode tensor $\mathcal{X} \in \mathbb{R}^{I_1 \times \cdots \times I_N}$, the rank- R CP decomposition of \mathcal{X} is an approximation

$$\mathcal{X} \approx \sum_{r=1}^R \lambda_r \mathbf{a}_r^{(1)} \circ \mathbf{a}_r^{(2)} \circ \cdots \circ \mathbf{a}_r^{(N)}, \quad (4)$$

where $\mathbf{a}_r^{(n)} \in \mathbb{R}^{I_n}$ are unit vectors with weight λ_r , and \circ denotes the outer product. The matrix formed by all the $\mathbf{a}_r^{(n)}$ vectors is called the factor matrix, that is, $\mathbf{A}^{(n)} = [\mathbf{a}_1^{(n)} \quad \mathbf{a}_2^{(n)} \quad \cdots \quad \mathbf{a}_r^{(n)}]$. So the CP decomposition can also be denoted by

$$\mathcal{X} \approx \left[\left[\lambda : \mathbf{A}^{(1)}, \mathbf{A}^{(2)}, \dots, \mathbf{A}^{(N)} \right] \right], \quad (5)$$

where $\lambda \in \mathbb{R}^R$ denotes the weight vector.

2.3 CP-ALS

The ALS [7, 15] is the most widely used CP decomposition algorithm. The core idea of this algorithm is to update one factor matrix at a time while keeping the others fixed. For the n th factor matrix, the ALS algorithm iteratively updates by solving the following quadratic subproblem:

$$\min_{\hat{\mathbf{A}}^{(n)}} \left\| \mathbf{X}_{(n)} - \hat{\mathbf{A}}^{(n)} \mathbf{P}^{(n)T} \right\|_F, \quad (6)$$

where $\hat{\mathbf{A}}^{(n)} = \mathbf{A}^{(n)} \cdot \text{diag}(\lambda)$ and $\mathbf{X}_{(n)}$ denotes the mode- n unfolding of the tensor $\mathcal{X} \in \mathbb{R}^{I_1 \times \cdots \times I_N}$. The $\mathbf{P}^{(n)} \in \mathbb{R}^{W_n \times R}$, where $W_n = I_1 \times \cdots \times I_{n-1} \times I_{n+1} \times \cdots \times I_N$ and R is the approximative rank of the \mathcal{X} , is formed by the Khatri-Rao product of the other factor matrices.

$$\mathbf{P}^{(n)} = \mathbf{A}^{(1)} \odot \cdots \odot \mathbf{A}^{(n-1)} \odot \mathbf{A}^{(n+1)} \odot \cdots \odot \mathbf{A}^{(N)}. \quad (7)$$

The subproblem (6) can be transformed into the following form:

$$\hat{\mathbf{A}}^{(n)} \mathbf{P}^{(n)T} = \mathbf{X}_{(n)}. \quad (8)$$

To compute $\hat{\mathbf{A}}^{(n)}$, we need to solve the linear system defined in (8). However, since $\mathbf{P}^{(n)T}$ is not a square matrix, it does not have a direct inverse. To address this, we pre-multiply both sides of (8) by $\mathbf{P}^{(n)}$, forming the normal equation. This results in a symmetric positive semi-definite system involving the square matrix $\mathbf{\Gamma}^{(n)}$, which can be efficiently inverted if it is well-conditioned. Consequently, by (8), we derive

$$\hat{\mathbf{A}}^{(n)} \mathbf{\Gamma}^{(n)} = \mathbf{X}_{(n)} \mathbf{P}^{(n)}, \quad (9)$$

where $\mathbf{\Gamma}^{(n)} \in \mathbb{R}^{R \times R}$ can be computed via

$$\mathbf{\Gamma}^{(n)} = \mathbf{S}_1 * \cdots * \mathbf{S}_{n-1} * \mathbf{S}_{n+1} * \cdots * \mathbf{S}_N, \quad (10)$$

where $\mathbf{S}_i = (\mathbf{A}^{(i)})^T \mathbf{A}^{(i)}$, $i = 1, \dots, n-1, n+1, \dots, N$.

By multiplying both sides of (9) by $\mathbf{\Gamma}^{(n)-1}$, we obtain $\hat{\mathbf{A}}^{(n)}$. Subsequently, normalizing the columns of $\hat{\mathbf{A}}^{(n)}$ yields the factor matrix $\mathbf{A}^{(n)}$. The detailed implementation of the ALS algorithm is provided in Algorithm 1.

Algorithm 1 CP-ALS

Input: Tensor $\mathcal{X} \in \mathbb{R}^{I_1 \times \cdots \times I_N}$, rank R , stopping criteria ϵ , iteration count m .

Initialize: Factor matrices $\mathbf{A}^{(1)}, \dots, \mathbf{A}^{(N)}$, gram matrices $\mathbf{S}_1 = (\mathbf{A}^{(1)})^T \mathbf{A}^{(1)}, \dots, \mathbf{S}_N = (\mathbf{A}^{(N)})^T \mathbf{A}^{(N)}$.

- 1: **for** $k = 0, 1, \dots, m$ **do**
- 2: **for** $n = 1, 2, \dots, N$ **do**
- 3: $\mathbf{\Gamma}^{(n)} = \mathbf{S}_1 * \cdots * \mathbf{S}_{n-1} * \mathbf{S}_{n+1} * \cdots * \mathbf{S}_N$.
- 4: $\mathbf{P}^{(n)} = \mathbf{A}^{(1)} \odot \cdots \odot \mathbf{A}^{(n-1)} \odot \mathbf{A}^{(n+1)} \odot \cdots \odot \mathbf{A}^{(N)}$.
- 5: $\mathbf{M}_n = \mathbf{X}_{(n)} \mathbf{P}^{(n)}$.
- 6: Solve $\hat{\mathbf{A}}^{(n)} \mathbf{\Gamma}^{(n)} = \mathbf{M}_n$ to obtain $\hat{\mathbf{A}}^{(n)}$.
- 7: Normalize columns of $\hat{\mathbf{A}}^{(n)}$ to obtain factor matrix $\mathbf{A}^{(n)}$.
- 8: Recompute gram matrix $\mathbf{S}_n = (\mathbf{A}^{(n)})^T \mathbf{A}^{(n)}$ for updated factor matrix $\mathbf{A}^{(n)}$.
- 9: **end for**
- 10: Compute the *fitness*.
- 11: **if** $\text{fitness} \geq \epsilon$ **then**
- 12: Break
- 13: **end if**
- 14: **end for**

Output: Matrices $\{\mathbf{A}^{(1)} \dots \mathbf{A}^{(N)}\}$.

2.4 CP-ALS-QR

The CP-ALS algorithm solves the linear system in (8) using the normal equation, which involves forming $\mathbf{\Gamma}^{(n)} = \mathbf{P}^{(n)} \mathbf{P}^{(n)T}$ and explicitly computing its inverse. In contrast, the CP-ALS-QR variant [24] improves numerical stability by replacing the normal equation approach with QR decomposition, thereby avoiding direct matrix inversion.

The transformation of $\mathbf{P}^{(n)T}$ is carried out as follows: First, we compute the compact QR factorization of each individual factor matrix, such that $\mathbf{A}^{(i)} = \mathbf{Q}_i \mathbf{R}_i$. Consequently, $\mathbf{P}^{(n)}$ can be reformulated in the following manner:

$$\begin{aligned} \mathbf{P}^{(n)} &= \mathbf{A}^{(N)} \odot \cdots \odot \mathbf{A}^{(n+1)} \odot \mathbf{A}^{(n-1)} \odot \cdots \odot \mathbf{A}^{(1)} \\ &= \mathbf{Q}_N \mathbf{R}_N \odot \cdots \odot \mathbf{Q}_{n+1} \mathbf{R}_{n+1} \odot \mathbf{Q}_{n-1} \mathbf{R}_{n-1} \odot \cdots \odot \mathbf{Q}_1 \mathbf{R}_1 \\ &= (\mathbf{Q}_N \otimes \cdots \otimes \mathbf{Q}_{n+1} \otimes \mathbf{Q}_{n-1} \otimes \cdots \otimes \mathbf{Q}_1) \underbrace{(\mathbf{R}_N \odot \cdots \odot \mathbf{R}_{n+1} \odot \mathbf{R}_{n-1} \odot \cdots \odot \mathbf{R}_1)}_{\mathbf{Z}_n}, \end{aligned} \quad (11)$$

where the last equality follows from (1). Second, we compute the QR decomposition of the matrix $\mathbf{Z}_n = \mathbf{Q}_0 \mathbf{R}_0$. Thus, we have

$$\begin{aligned} \mathbf{P}^{(n)} &= (\mathbf{Q}_N \otimes \cdots \otimes \mathbf{Q}_{n-1} \otimes \mathbf{Q}_{n+1} \otimes \cdots \otimes \mathbf{Q}_1) (\mathbf{R}_1 \odot \cdots \odot \mathbf{R}_{n-1} \odot \mathbf{R}_{n+1} \odot \cdots \odot \mathbf{R}_N) \\ &= \underbrace{(\mathbf{Q}_N \otimes \cdots \otimes \mathbf{Q}_{n+1} \otimes \mathbf{Q}_{n-1} \otimes \cdots \otimes \mathbf{Q}_1)}_{\mathbf{Q}} \underbrace{\mathbf{Q}_0 \mathbf{R}_0}_{\mathbf{R}}, \end{aligned} \quad (12)$$

where \mathbf{Q} has orthonormal columns, and \mathbf{R} is upper triangular.

By applying the aforementioned QR decomposition to $\mathbf{P}^{(n)T}$, linear system (8) can be reformulated as follows:

$$\hat{\mathbf{A}}^{(n)} \mathbf{R}^T \mathbf{Q}^T = \mathbf{X}_{(n)}, \quad (13)$$

where $\mathbf{Q} = (\mathbf{Q}_N \otimes \cdots \otimes \mathbf{Q}_{n+1} \otimes \mathbf{Q}_{n-1} \otimes \cdots \otimes \mathbf{Q}_1) \mathbf{Q}_0$, $\mathbf{R} = \mathbf{R}_0$. Given that the matrix \mathbf{Q} is orthonormal, it follows that $\mathbf{Q}^T \mathbf{Q} = \mathbf{I}$. Consequently, by multiplying both sides of (13) by \mathbf{Q} , we obtain

$$\hat{\mathbf{A}}^{(n)} \mathbf{R}^T = \mathbf{Y}_{(n)} \mathbf{Q}_0, \quad (14)$$

where $\mathbf{Y}_{(n)} = \mathbf{X}_{(n)} (\mathbf{Q}_N \otimes \cdots \otimes \mathbf{Q}_{n-1} \otimes \mathbf{Q}_{n+1} \otimes \cdots \otimes \mathbf{Q}_1)$. The $\mathbf{Y}_{(n)}$ is the mode- n unfolding of $\mathcal{Y} = \mathcal{X} \times_1 \mathbf{Q}_1^T \times_2 \cdots \times_{i-1} \mathbf{Q}_{i-1}^T \times_{i+1} \mathbf{Q}_{i+1}^T \times_{n+2} \cdots \times_N \mathbf{Q}_N^T$. By transposing (14) and solving the resulting system of linear equations, we obtain the matrix $\hat{\mathbf{A}}^{(n)}$. Then, we normalize its columns to derive $\mathbf{A}^{(n)}$. The detailed implementation of ALS-QR is presented in Algorithm 2.

Algorithm 2 CP-ALS-QR

Input: Tensor $\mathcal{X} \in \mathbb{R}^{I_1 \times \cdots \times I_N}$, rank R , stopping criteria ϵ , iteration count m .

Initialize: Factor matrices $\mathbf{A}^{(1)} \cdots \mathbf{A}^{(N)}$, calculate QR-decomposition $\mathbf{Q}_1 \mathbf{R}_1 \cdots \mathbf{Q}_N \mathbf{R}_N$ of factor matrices.

- 1: **for** $k = 0, 1, \dots, m$ **do**
- 2: **for** $n = 1, 2, \dots, N$ **do**
- 3: $\mathbf{Z}_n = \mathbf{R}_N \odot \cdots \odot \mathbf{R}_{n+1} \odot \mathbf{R}_{n-1} \odot \cdots \odot \mathbf{R}_1$.
- 4: Calculate QR decomposition $\mathbf{Z}_n = \mathbf{Q}_0 \mathbf{R}_0$.
- 5: $\mathcal{Y} = \mathcal{X} \times_1 \mathbf{Q}_1^T \times_2 \cdots \times_{n-1} \mathbf{Q}_{n-1}^T \times_{n+1} \mathbf{Q}_{n+1}^T \times_{n+2} \cdots \times_N \mathbf{Q}_N^T$.
- 6: $\mathbf{V}_n = \mathbf{Y}_{(n)} \mathbf{Q}_0$.
- 7: Solve $\hat{\mathbf{A}}^{(n)} \mathbf{R}_0^T = \mathbf{V}_n$ to obtain $\hat{\mathbf{A}}^{(n)}$.
- 8: Normalize columns of $\hat{\mathbf{A}}^{(n)}$ to obtain factor matrix $\mathbf{A}^{(n)}$.
- 9: Recompute QR-decomposition for updated factor matrix $\mathbf{A}^{(n)} = \mathbf{Q}_n \mathbf{R}_n$.
- 10: **end for**
- 11: Compute the *fitness*.
- 12: **if** $\text{fitness} \geq \epsilon$ **then**
- 13: Break
- 14: **end if**
- 15: **end for**

Output: Matrices $\{\mathbf{A}^{(1)} \cdots \mathbf{A}^{(N)}\}$.

3 Branch reutilization of dimension tree and extrapolation

In this section, we introduce the branch reutilization of dimension tree and the extrapolation design for matrix \mathbf{Q}_0 in line 4 of Algorithm 2. Based on these techniques, we develop an ALS-QR-BRE algorithm for the CP decomposition. Additionally, we give a complexity analysis of the branch reutilization of dimension tree.

3.1 Branch reutilization of dimension tree

The dimension tree provides a hierarchical partitioning of mode indices in an N -dimensional tensor, enabling more efficient computation in tensor decomposition. Originally, it was introduced to facilitate hierarchical Tucker decomposition [14], which offers a structured way to represent tensors while reducing computational complexity. Compared to the conventional Tucker decomposition, the dimension tree approach is particularly advantageous for high-order tensors, where direct Tucker decomposition becomes impractical due to its high computational cost. A key component of the

dimension tree structure is the intermediate tensors, which are partially contracted TTMC tensors. These intermediate tensors, denoted as $\mathcal{Y}^{(i_1, i_2, \dots, i_m)}$, are defined as follows:

$$\mathcal{Y}^{(i_1, i_2, \dots, i_m)} = \mathcal{X} \times_{n \in \{1, 2, \dots, N\} \setminus \{i_1, i_2, \dots, i_m\}} \mathbf{A}_n^T, \quad (15)$$

where \mathcal{X} is contracted with all the matrices \mathbf{A}_n except $\mathbf{A}_{i_1}, \dots, \mathbf{A}_{i_m}$. The \mathbf{A}_n is with respect to \mathbf{Q}_n in line 5 of Algorithm 2. Building upon the definition of TTMC delineated in (15), the dimension trees for third-order and fourth-order tensors are depicted schematically in Figure 1.

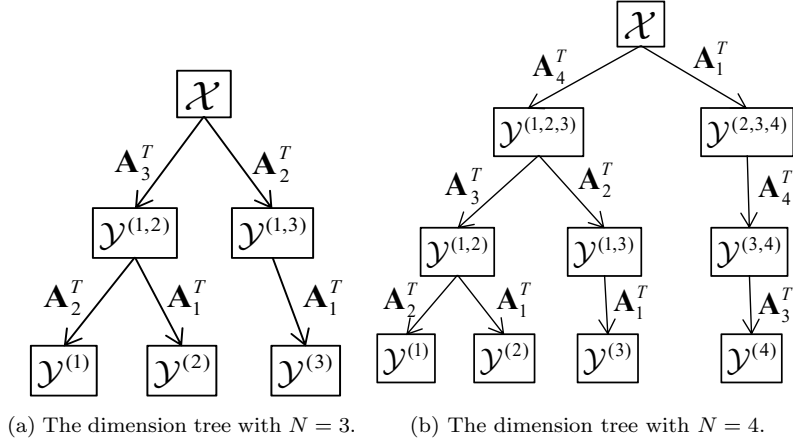


Figure 1: The canonical dimension tree architecture of third-order and fourth-order tensors.

As shown in Figure 1, the dimension tree structure does not fully exploit certain intermediate tensors during the iteration process, leading to inefficiencies. For instance, in Figure 1(a), the tensor $\mathcal{Y}^{(1,3)}$ remains unexploited to updating the factor matrix $\mathbf{A}^{(1)}$, which results in unnecessary memory usage. To address this issue, we introduce branch reutilization of dimension tree, which improves computational efficiency by making better use of intermediate tensors. The key principles of this approach are maximizing the reuse of intermediate tensors, ensuring that previously computed tensors are effectively utilized in subsequent iterations, and reducing reliance on the original tensor by using intermediate tensors to update factor matrices associated with different indices, minimizing the need to repeatedly access the original tensor. Figure 2 illustrates which intermediate tensors are not fully utilized during the iteration process.

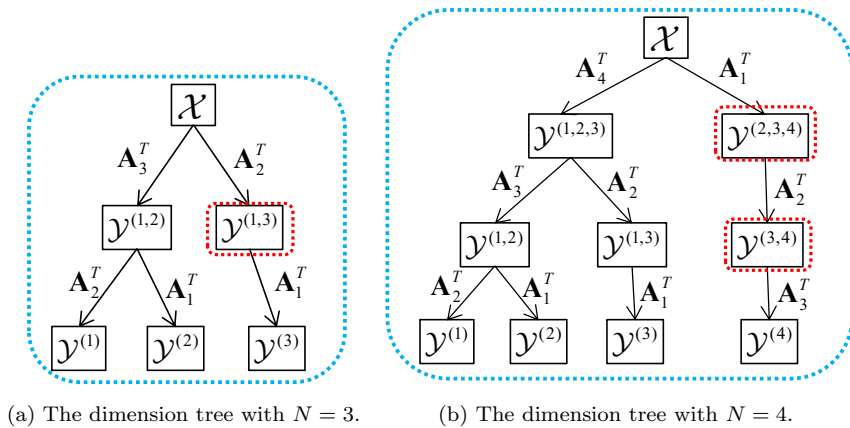


Figure 2: The tensor that remains underutilized is emphasized within the red-dashed box. (a) Shows the underutilized tensor $\mathcal{Y}^{(1,3)}$. (b) Shows the underutilized tensors $\mathcal{Y}^{(3,4)}$ and $\mathcal{Y}^{(2,3,4)}$.

In the case of third-order tensors, unlike the traditional dimension tree, which repeatedly applies the same structural approach, the proposed branch reutilization method starts the second iteration from the underutilized tensor $\mathcal{Y}^{(1,3)}$. By the third iteration, all tensors have been fully utilized, eliminating the need to access underutilized tensors. Consequently, rather than restarting from the original tensor, the iteration proceeds directly from the intermediate tensor $\mathcal{Y}^{(2,3)}$. If the third iteration were to begin from the original tensor, an additional TTM computation would be required every two iterations, compared to starting from an intermediate tensor. Therefore, to minimize computational overhead, it is more efficient to avoid restarting iterations from the original tensor. Figure 3 illustrates the branch reutilization method for third-order tensors.

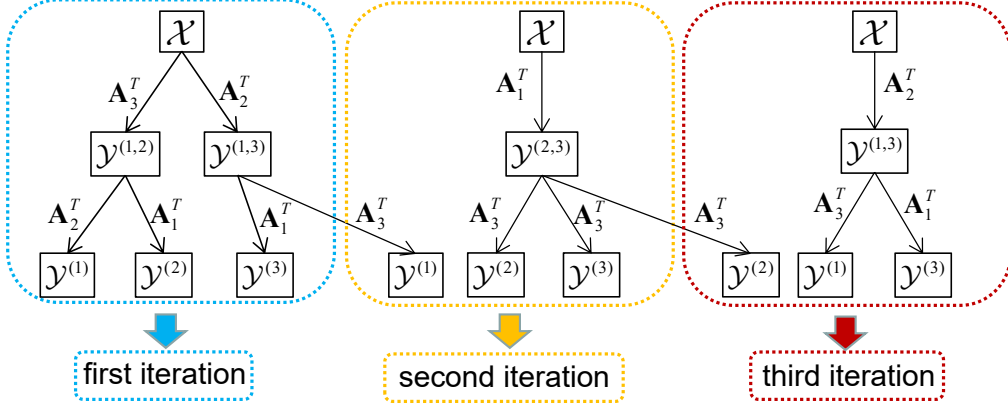


Figure 3: The iterative structure of branch reutilization of dimension tree for third-order tensor.

For fourth-order tensors, the branch reutilization of dimension tree updates iteratively by combining intermediate tensors with underutilized ones. In each iteration, we prioritize reusing underutilized tensors to compute the corresponding factor matrices. In the second iteration, the intermediate tensor $\mathcal{Y}^{(3,4)}$, generated in the first iteration, remains unused for updating $\mathbf{A}^{(3)}$, so the second iteration begins from $\mathcal{Y}^{(3,4)}$. By the third iteration, the intermediate tensor $\mathcal{Y}^{(1,3,4)}$ from the second iteration is still underutilized and not yet applied to compute $\mathbf{A}^{(3)}$. Therefore, the third iteration begins by utilizing $\mathcal{Y}^{(1,4)}$ to update $\mathbf{A}^{(1)}$, followed by the use of $\mathcal{Y}^{(1,3,4)}$ to compute $\mathbf{A}^{(3)}$. Figure 4 illustrates the refined iterative structure for the branch reutilization of dimension tree in the fourth-order case.

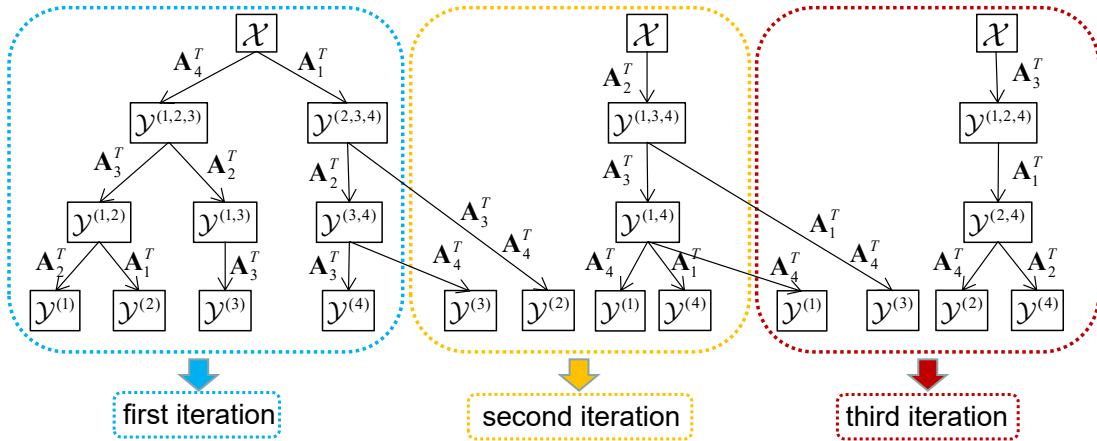


Figure 4: The iterative structure of branch reutilization of dimension tree for fourth-order tensor.

In this subsection, we present a comprehensive depiction of the branch reutilization of dimension tree. The core principle driving the construction of this method is based on alternating iterative updates of the factor matrices, wherein the branch reutilization of dimension tree systematically performs alternating updates of the factor matrices on the intermediate tensors.

3.2 Extrapolation

Extrapolation acceleration techniques [27] are well-studied methods for improving the efficiency of iterative optimization algorithms and have been extensively used in the field of convex optimization. In recent years, significant progress has been made in incorporating extrapolation strategies into the CP-ALS algorithm. Notable approaches include line search methods [5], momentum-based techniques [25], and block momentum acceleration [10]. These methods accelerate convergence by leveraging information from previous iterations to refine the current solution, thereby enhancing the overall optimization process. Next, we briefly review two commonly used extrapolation strategies.

Within the line search (LS) [5], at each iteration, an improved solution estimate is computed using an extrapolation mechanism. Formally, at iteration k , the solution is obtained as a combination of the current iterate \mathbf{x}_k and the previous iterate \mathbf{x}_{k-1} , weighted by an extrapolation parameter β_k , as follows

$$\mathbf{x}_{k+1}^{(new)} = \mathbf{x}_{k-1} + \beta_k(\mathbf{x}_k - \mathbf{x}_{k-1}), \quad (16)$$

where $\mathbf{x}_{k+1}^{(new)}$ represents a vector comprising the elements of the factor matrices $\mathbf{A}^{(1)}, \dots, \mathbf{A}^{(N)}$. If $\mathbf{x}_{k+1}^{(new)}$ yields a lower reconstruction error compared to \mathbf{x}_{k-1} , it is accepted as the updated solution, and the factor matrices are subsequently refined. Otherwise, $\mathbf{x}_{k+1}^{(new)}$ is discarded, and the factor matrices are updated following the standard CP-ALS algorithm. Various strategies exist for determining the step size β_k , including the cubic root rule $\sqrt[3]{k}$ [5] or a fixed value within the range of 1.2 to 1.3 [31].

Momentum ALS (M-ALS) [10] offers an alternative extrapolation strategy to standard line search and enhanced line search techniques. Unlike traditional methods, the M-ALS algorithm first applies an extrapolation step to predict an improved candidate solution based on previous iterates. This predicted solution then undergoes an ALS update to refine the estimate,

$$\mathbf{x}_{k+1}^{(new)} = q_{ALS}(\mathbf{x}_k + \beta_k(\mathbf{x}_k - \mathbf{x}_{k-1})). \quad (17)$$

If $\mathbf{x}_{k+1}^{(new)}$ yields a reconstruction error smaller than that of \mathbf{x}_k , it is accepted as the new candidate solution. Otherwise, it is discarded and a standard ALS step is applied to \mathbf{x}_k .

Building on the above work, we propose introducing an extrapolation strategy to enhance the numerical efficiency of Algorithm 2, which is implemented in line 4 of Algorithm 2, as follows

$$\hat{\mathbf{Q}}_0^k = \mathbf{Q}_0^k + \beta_k(\mathbf{Q}_0^k - \mathbf{Q}_0^{k-1}). \quad (18)$$

However, empirical analysis reveals that this extrapolation mechanism has limited effectiveness in enhancing tensor approximation accuracy due to the inherent structural constraints of \mathbf{Q}_0 . Specifically, \mathbf{Q}_0 has a unique structure where the first element in its first row and first column is 1, while all other elements in the first row and first column are 0. Consequently, the extrapolation operation (18) leaves the first row and first column of \mathbf{Q}_0 , which significantly limits the effectiveness of extrapolation. To address this limitation, we develop a refined extrapolation approach that better accommodates the structure of \mathbf{Q}_0 . The modified extrapolation step is as follows:

$$\hat{\mathbf{Q}}_0^k = \mathbf{Q}_0^k + \beta(\mathbf{Q}_0^k - \alpha\mathbf{Q}_0^{k-1}), \quad (19)$$

where β and α represent tunable hyperparameters. Unlike the traditional extrapolation (16), the modified form (19) slightly reduces acceleration but enhances numerical stability and better aligns with the structural constraints of \mathbf{Q}_0 .

3.3 ALS-QR-BRE

Through integrating the optimized dimension tree architecture (see Subsection 3.1) and the extrapolation strategy (see Subsection 3.2), we propose a novel algorithm, ALS-QR-BRE. This algorithm is based on two key principles: (i) the branch reutilization of dimension tree accelerates computations in line 5 of Algorithm 2, leading to improved computational efficiency; (ii) the extrapolation technique is applied to matrix \mathbf{Q}_0 in line 4 of Algorithm 2 to enhance approximation accuracy. The full implementation is provided in Algorithm 3.

Algorithm 3 ALS-QR-BRE

Input: Tensor $\mathcal{X} \in \mathbb{R}^{I_1 \times \dots \times I_N}$, rank R , stopping criteria ϵ , iteration count m .

Initialize: Factor matrices $\mathbf{A}^{(1)} \dots \mathbf{A}^{(N)}$, calculate QR-decomposition $\mathbf{Q}_1 \mathbf{R}_1, \dots, \mathbf{Q}_N \mathbf{R}_N$ of factor matrices.

```

1: for  $k = 0, 1, \dots, m$  do
2:   for  $n = 1, 2, \dots, N$  do
3:      $\mathbf{Z}_n = \mathbf{R}_N \odot \dots \odot \mathbf{R}_{n+1} \odot \mathbf{R}_{n-1} \odot \dots \odot \mathbf{R}_1$ .
4:     Calculate QR-decomposition  $\mathbf{Z}_n = \mathbf{Q}_0^k \mathbf{R}_0$ .
5:      $\hat{\mathbf{Q}}_0^k = \mathbf{Q}_0^k + \beta(\mathbf{Q}_0^k - \alpha \mathbf{Q}_0^{k-1})$ . ← Subsection 3.2
6:     Calculate  $\mathcal{Y}$  using the branch reutilization of dimension tree. ← Subsection 3.1
7:      $\mathbf{V}_n = \mathbf{Y}_{(n)} \hat{\mathbf{Q}}_0^k$ .
8:     Solve  $\hat{\mathbf{A}}^{(n)} \mathbf{R}_0^T = \mathbf{V}_n$  to obtain  $\hat{\mathbf{A}}^{(n)}$ .
9:     Normalize columns of  $\hat{\mathbf{A}}^{(n)}$  to obtain factor matrix  $\mathbf{A}^{(n)}$ .
10:    Recompute QR-decomposition for updated factor matrix  $\mathbf{A}^{(n)} = \mathbf{Q}_n \mathbf{R}_n$ .
11:  end for
12:  Compute the fitness.
13:  if  $fitness \geq \epsilon$  then
14:    Break
15:  end if
16: end for

```

Output: Matrices $\{\mathbf{A}^{(1)}, \dots, \mathbf{A}^{(N)}\}$.

At the initial stage of the Algorithm 3, if the discrepancy between the fitted values in the first two iterations is large, the extrapolation operation for \mathbf{Q}_0 in line 5 is temporarily omitted to prevent excessive fluctuations. During this phase, the Algorithm 3 reduces to ALS-QR-BR, performing iterative tensor computation without extrapolation. Once the variation between successive fitted values falls below a predefined threshold, the extrapolation is activated, accelerating convergence and improving both computational efficiency and fitting accuracy.

3.4 Complexity analysis

The complexity analysis primarily focuses on optimizing multiple TTM operations through branch reutilization of dimension tree. To evaluate its effectiveness in reducing computational complexity, we compare three computational scenarios over the first three iterations:

- Without the dimension tree (unoptimized contraction ordering, equivalent to line 5 of Algorithm 2).
- Standard dimension tree (hierarchical decomposition).
- Branch reutilization of dimension tree (corresponding to line 6 of Algorithm 3).

We derive theoretical complexity bounds for these three cases, focusing on the cumulative computational cost of line 6 in Algorithm 3 during the first three iterations. The complexity of other steps

in Algorithm 3 has been analyzed in [24] and is not repeated here. Our study considers third-order and fourth-order tensors, as extending the analysis to higher-order cases under branch reutilization is significantly more complex and beyond the scope of this work.

To clarify the computational complexity of sequential TTM operations, we consider a third-order tensor $\mathcal{X} \in \mathbb{R}^{I_1 \times I_2 \times I_3}$ with the CP decomposition rank R . The first TTM along mode-1 incurs a computational cost of $2I_1I_2I_3R$, followed by the second TTM along mode-2 with a cost of $2I_2I_3R^2$, and the third TTM along mode-3 requires $2I_3R^3$ operations. By extending this pattern, we derive the subsequent computational complexity results presented in the figures and tables.

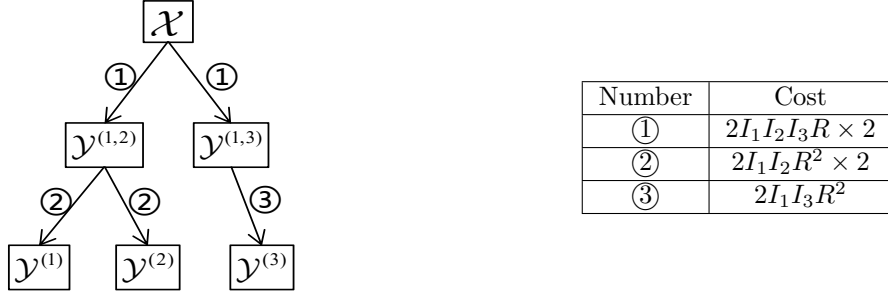


Table 1: The left diagram depicts the iterative structure of the dimension tree for third-order tensor, while the right table summarizes the total computational complexity per iteration. Identical-index edges indicate equivalent computational complexity.

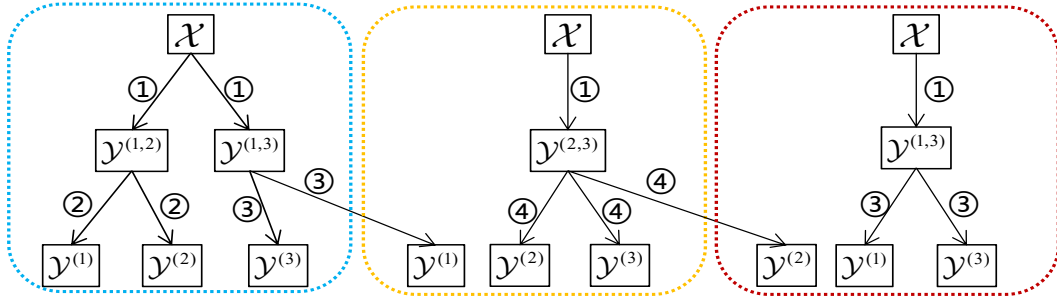


Figure 5: The iterative structure of branch reutilization of the dimension tree for third-order tensor. Edges with the same index represent the same computational complexity.

Table 2: The total computational cost required for each index.

Number	①	②	③	④
Cost	$2I_1I_2I_3R \times 4$	$2I_1I_2R^2 \times 2$	$2I_1I_3R^2 \times 4$	$2I_2I_3R^2 \times 3$

Through synthesizing the iterative complexities of the dimension tree (Table 1), the branch reutilization of dimension tree (Table 2), and the theoretical foundations of TTM complexity, we analytically derive the total computational complexity for the first three iterations of a third-order tensor across the three scenarios presented in Table 3.

Table 3: Computational complexity of three scenarios of third-order tensor.

Scenario	without the dimension tree	dimension tree	branch reutilization of dimension tree
Cost	$18I_1I_2I_3R + 6I_1I_2R^2 + 6I_2I_3R^2 + 6I_1I_3R^2$	$12I_1I_2I_3R + 12I_1I_2R^2 + 6I_1I_3R^2$	$8I_1I_2I_3R + 4I_1I_2R^2 + 8I_1I_3R^2 + 6I_2I_3R^2$

When $I_1 = I_2 = I_3$, the term $I_1 I_2 I_3 R$ dominates the overall computational cost. From the quantity of this term, we can conclude that the branch reutilization of dimension tree significantly reduces computational complexity compared to the scenario without the dimension tree, while also outperforming the use of the dimension tree.

Let $\mathcal{X} \in \mathbb{R}^{I_1 \times I_2 \times I_3 \times I_4}$ be a fourth-order tensor, and assume the CP approximation rank of R . By leveraging the theoretical framework TTM complexity, we derive the results presented in Table 4.

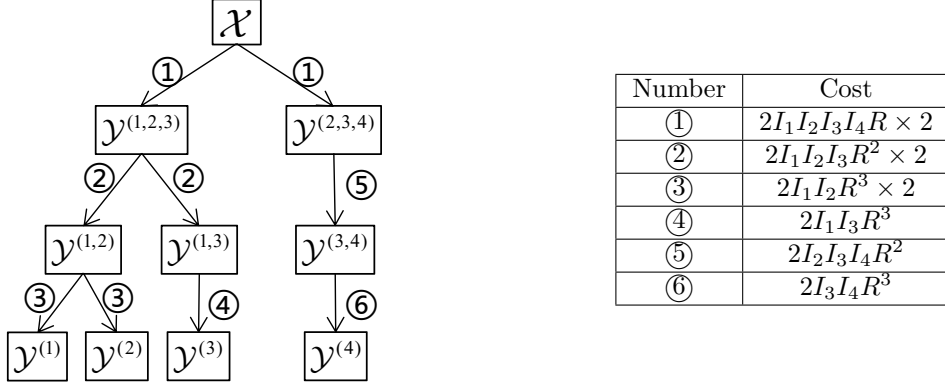


Table 4: The left diagram illustrates the iterative structure of the dimension tree for a fourth-order tensor, while the table on the right summarizes the corresponding computational complexity of each index in the dimension tree.

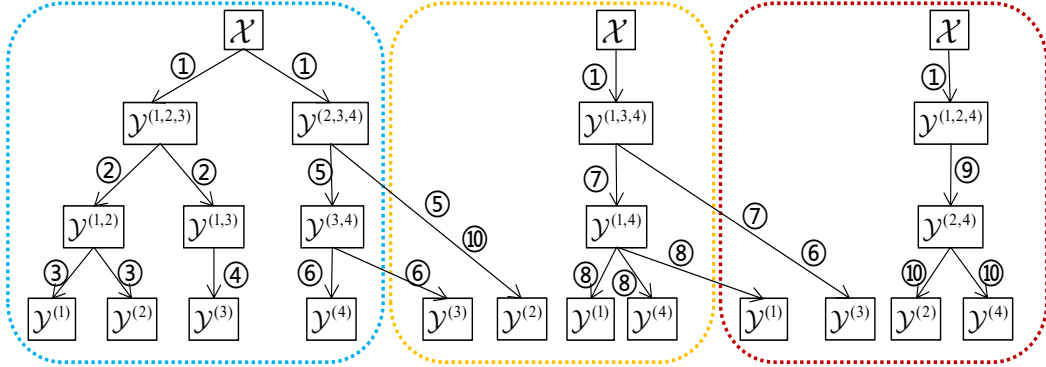


Figure 6: The iterative structure of branch reutilization of the dimension tree for fourth-order tensor. Edges with the same index represent the same computational complexity.

Table 5: The computational cost for each index of branch reutilization of dimension tree.

Number	①	②	③	④	⑤
Cost	$2I_1 I_2 I_3 I_4 R \times 4$	$2I_1 I_2 I_3 R^2 \times 2$	$2I_1 I_2 R^3 \times 2$	$2I_1 I_3 R^3$	$2I_2 I_3 I_4 R^2 \times 2$
Number	⑥	⑦	⑧	⑨	⑩
Cost	$2I_3 I_4 R^3 \times 3$	$2I_1 I_3 I_4 R^2 \times 2$	$2I_1 I_4 R^3 \times 3$	$2I_1 I_2 I_4 R^2$	$2I_2 I_4 R^3 \times 3$

By combining the iterative complexity of the dimension tree (Table 4), the complexity of the branch reutilization of dimension tree (Table 5), and the TTM complexity framework, we systematically derive the total computational complexity for the three scenarios, as shown in Table 6.

Table 6: Computational complexity of three scenarios of fourth-order tensor.

Scenario	without the dimension tree	dimension tree	branch reutilization of dimension tree
Cost	$24I_1I_2I_3I_4R + 12I_1I_2I_3R^2 + 12I_2I_3I_4R^2 + 12I_1I_2R^3 + 12I_3I_4R^3$	$12I_1I_2I_3I_4R + 12I_1I_2I_3R^2 + 6I_2I_3I_4R^2 + 12I_1I_2R^3 + 6I_1I_3R^3 + 6I_3I_4R^3$	$8I_1I_2I_3I_4R + 4I_2I_4R^3 + 6I_1I_4R^3 + 2I_1I_3R^3 + 4I_3I_4R^3 + 4I_1I_2R^3 + 2I_2I_3R^3 + 4I_1I_3I_4R^2 + 2I_1I_2I_4R^2 + 2I_3I_4R^3 + 4I_2I_3I_4R^2 + 4I_1I_2I_3R^2$

When $I_1 = I_2 = I_3 = I_4$, the dominant computational cost is $I_1I_2I_3I_4R$. In branch reutilization of the dimension tree, the occurrence of this term is fewer compared to both the classical dimension tree and without the dimension tree. Consequently, the computational cost of the branch reutilization of dimension tree is lower than that of the other two scenarios.

The above analysis presents the total computational cost over the first three iterations for third-order and fourth-order tensors under three different scenarios: without the dimension tree, dimension tree, and branch reutilization of dimension tree. By comparing the main computational terms, we find that the branch reutilization of dimension tree results in lower computational cost.

4 Numerical experiments

In this section, we evaluate the performance of our proposed algorithms, ALS-QR-BRE and ALS-QR-BR, on random, synthetic, and real tensors, and compare them with the classical CP-ALS [7], CP-ALS-PINV, as well as the unmodified CP-ALS-QR [24] and CP-ALS-QR-SVD algorithms to assess their efficiency. All numerical experiments were conducted on a PC with an i7-12700 processor, 16 GB of RAM, and implemented in MATLAB using Tensortoolbox [4] and Tensorlab [15]. A comparison of each algorithm is provided in the table 7. This implementation will be made available at <https://github.com/youmengx658/ALS-QR-BRE> upon acceptance of this manuscript.

Table 7: Algorithm.

Name	Interpretation
CP-ALS (ALS)	Algorithm 1 (line 6) with Cholesky for the inverse.
CP-ALS-PINV (PINV)	Algorithm 1 (line 6) with SVD for the inverse.
CP-ALS-QR (QR)	Algorithm 2.
CP-ALS-QR-SVD (QR-SVD)	Algorithm 2 (line 7) with SVD for the inverse.
CP-ALS-QR-DT (QR-DT)	Algorithm 2 (line 6) with the dimension tree.
ALS-QR-BR(QR-BR)	Algorithm 3 with $\beta = 0$.
ALS-QR-BRE (QR-BRE)	Algorithm 3.

The abbreviations in parentheses in Table 7 represent the algorithms used for the evaluation of the average iteration time in Subsection 4.2. The full names of the algorithms are employed in the experiments involving synthetic and real tensors, as discussed in Subsections 4.3 and 4.4.

4.1 Approximation error

The following experiments are conducted based on the approximation error defined as follows:

$$\sqrt{\|\mathcal{X} - \mathcal{K}\|^2} = \sqrt{\|\mathcal{X}\|^2 - 2\langle \mathcal{X}, \mathcal{K} \rangle + \|\mathcal{K}\|^2},$$

where $\|\mathcal{X}\|^2$ is precomputed and remains constant throughout the iteration process. $\langle \mathcal{X}, \mathcal{K} \rangle$ and $\|\mathcal{K}\|^2$ are computed using intermediate quantities generated during algorithm iterations.

In the CP-ALS algorithm, the approximation \mathcal{K} is expressed as $\mathbf{K}_{(n)} = \hat{\mathbf{A}}^{(n)}\mathbf{P}^{(n)T}$, where $\hat{\mathbf{A}}^{(n)} = \mathbf{A}^{(n)} \cdot \text{diag}(\lambda)$ and $\mathbf{P}^{(n)} = \mathbf{A}^{(1)} \odot \dots \odot \mathbf{A}^{(n-1)} \odot \mathbf{A}^{(n+1)} \odot \dots \odot \mathbf{A}^{(N)}$. Consequently, the inner product between the tensor \mathcal{X} and the approximation \mathcal{K} is given by:

$$\langle \mathcal{X}, \mathcal{K} \rangle = \langle \mathbf{X}_{(n)}, \mathbf{K}_{(n)} \rangle = \langle \mathbf{X}_{(n)}, \hat{\mathbf{A}}^{(n)}\mathbf{P}^{(n)T} \rangle = \langle \mathbf{X}_{(n)}\mathbf{P}^{(n)}, \hat{\mathbf{A}}^{(n)} \rangle = \langle \mathbf{M}_n, \hat{\mathbf{A}}^{(n)} \rangle,$$

where \mathbf{M}_n computed as described in line 5 of Algorithm 1. Similarly, the squared norm of \mathcal{K} is calculated as:

$$\|\mathcal{K}\|^2 = \langle \hat{\mathbf{A}}^{(n)}\mathbf{P}^{(n)T}, \hat{\mathbf{A}}^{(n)}\mathbf{P}^{(n)T} \rangle = \langle \mathbf{P}^{(n)T}\mathbf{P}^{(n)}, (\hat{\mathbf{A}}^{(n)})^T \hat{\mathbf{A}}^{(n)} \rangle = \langle \mathbf{\Gamma}^{(n)}, \text{diag}(\lambda)\mathbf{S}_n\text{diag}(\lambda) \rangle,$$

where $\mathbf{\Gamma}^{(n)}$ is computed in line 3 of Algorithm 1 and the $\mathbf{S}_n = (\mathbf{A}^{(n)})^T \mathbf{A}^{(n)}$ is gram matrix of the n th factor matrix. Typically, the index n refers to the last mode in the subiteration. This approach for calculating the approximation error is well-established in [4, 12, 22, 30, 35].

According to the previously described computation method, $\mathbf{K}_{(n)} = \hat{\mathbf{A}}^{(n)}\mathbf{P}^{(n)T}$ where $\mathbf{P}^{(n)} = (\mathbf{Q}_N \otimes \dots \otimes \mathbf{Q}_{n+1} \otimes \mathbf{Q}_{n-1} \otimes \dots \otimes \mathbf{Q}_1)\mathbf{Q}_0\mathbf{R}_0$ for the Algorithm 2. Consequently, the inner product between \mathcal{X} and \mathcal{K} is expressed as:

$$\langle \mathcal{X}, \mathcal{K} \rangle = \langle \mathbf{X}_{(n)}, \mathbf{K}_{(n)} \rangle = \langle \mathbf{X}_{(n)}, \hat{\mathbf{A}}^{(n)}\mathbf{P}^{(n)T} \rangle = \langle \mathbf{X}_{(n)}\mathbf{P}^{(n)}, \hat{\mathbf{A}}^{(n)} \rangle = \langle \mathbf{V}_n, \hat{\mathbf{A}}^{(n)}\mathbf{R}_0^T \rangle,$$

where \mathbf{V}_n is computed as outlined in line 6 of Algorithm 2, and \mathbf{R}_0 is the upper triangular matrix obtained from the QR decomposition in line 4 of Algorithm 2. Similarly, the squared norm of \mathcal{K} is given by:

$$\|\mathcal{K}\|^2 = \langle \hat{\mathbf{A}}^{(n)}\mathbf{P}^{(n)T}, \hat{\mathbf{A}}^{(n)}\mathbf{P}^{(n)T} \rangle = \langle \mathbf{P}^{(n)T}\mathbf{P}^{(n)}, (\hat{\mathbf{A}}^{(n)})^T \hat{\mathbf{A}}^{(n)} \rangle = \langle \mathbf{R}_0^T \mathbf{R}_0, \text{diag}(\lambda)\mathbf{R}_n^T \mathbf{R}_n \text{diag}(\lambda) \rangle,$$

where \mathbf{R}_n is the upper triangular matrix in the QR decomposition of $\mathbf{A}^{(n)}$. This error calculation approach for the CP-ALS-QR algorithm was initially introduced in [24]. The fitness metric, which evaluates the quality of the approximation, is defined as:

$$\text{Fitness} = 1 - \frac{\sqrt{\|\mathcal{X} - \mathcal{K}\|^2}}{\|\mathcal{X}\|},$$

where a fitness value approaching 1 indicates a better approximation of \mathcal{X} by \mathcal{K} .

4.2 Evaluate the average iteration time on random tensors

In this subsection, we conduct experiments on random tensors of orders three, four, five, and six to evaluate the impact of increasing rank on the average iteration time of each algorithm. Specifically, the dimensions of the third-order tensor are set to 700 for each mode, while those of the fourth-order, fifth-order, and sixth-order tensors are set to 150, 50, and 25, respectively. Each algorithm is executed 10 times. To minimize the influence of initialization bias, the runtime of the first execution is discarded, and the average runtime of the subsequent executions is computed. The experimental results for tensors of varying ranks across these four cases are presented in Figure 7.

As shown in Figure 7, MTTKRP and Gram (refer to lines 3 and 5 in Algorithm 1) represent the proportion of computational time spent on calculating $\mathbf{M}_i = \mathbf{X}_{(i)}\mathbf{P}^{(i)}$ and computing the Gram matrix for each factor matrix, respectively, within the ALS and PINV algorithms. TTM and QR denote the computational time consumed by TTM operations and QR decomposition in the QR, QR-SVD, QR-DT, and QR-BRE algorithms. Specifically, the TTM and QR operations correspond to lines 5 and initialize in Algorithm 2, as well as lines 6 and initialize in Algorithm 3. The computation of \mathbf{Q}_0 involves performing QR decomposition on the Khatri-Rao product \mathbf{Z}_n (refer to line 4 in Algorithms

2 and 3), while the application of \mathbf{Q}_0 corresponds to a matrix multiplication operation (refer to line 6 in Algorithm 2 and line 7 in Algorithm 3). Other steps, such as extrapolation, weight computation, and error calculation, are categorized as "other" due to their minimal contribution to the overall computational time. Since the time spent on extrapolation is negligible, the iteration time for the QR-BR algorithm is the same as that for QR-BRE. Additionally, for each rank, the runtime ratio between ALS and QR-BRE is highlighted in red, while the runtime ratio between ALS and QR is highlighted in black.

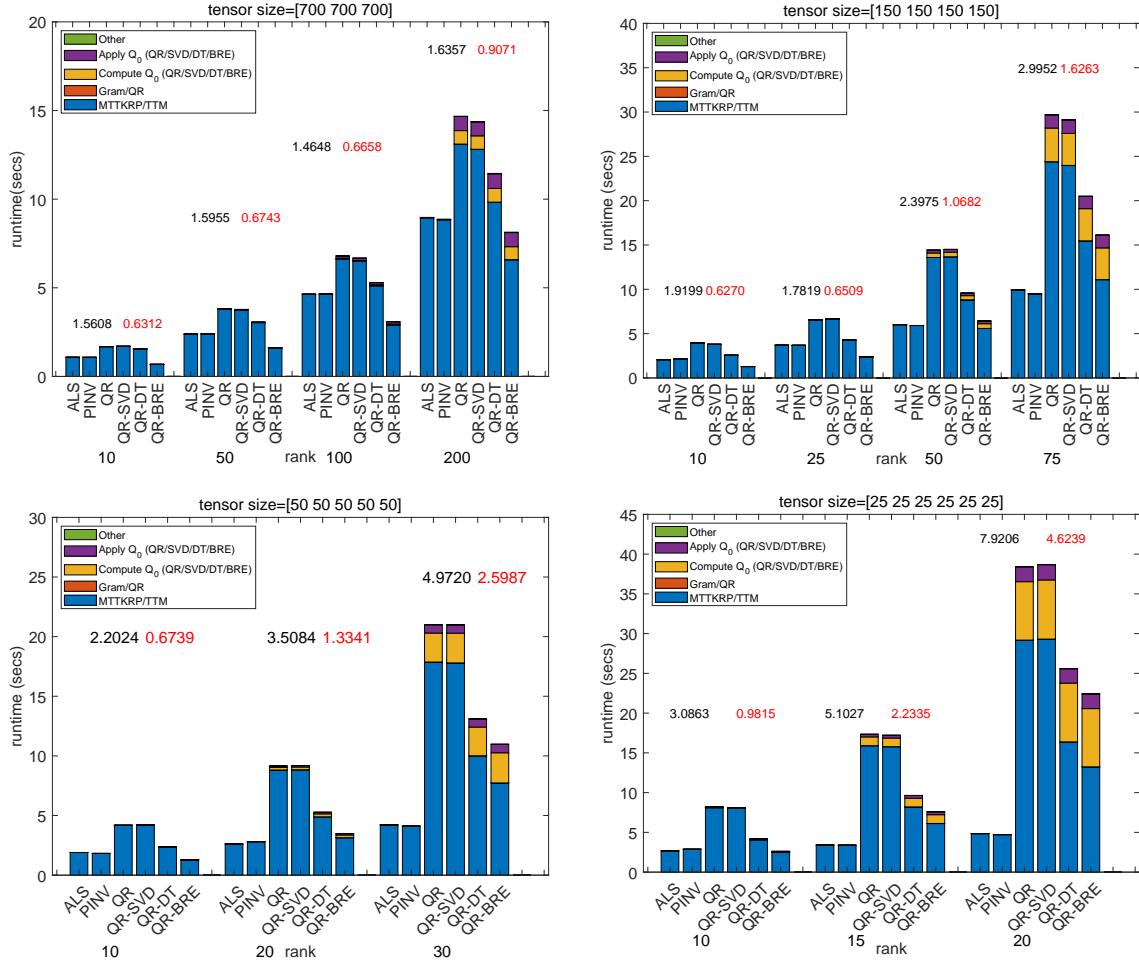


Figure 7: The average runtime (in seconds) for a single iteration of ALS, PINV, QR, QR-SVD, QR-DT, and QR-BRE is presented as the rank increases, for a third-order tensor of size 700 (top left), a fourth-order tensor of size 150 (top right), a five-order tensor of size 50 (bottom left), and a six-order tensor of size 25 (bottom right).

From the experimental results in Figure 7, it can be observed that the primary computational cost per iteration is MTKRP for the ALS and PINV algorithms, whereas for the QR, QR-SVD, QR-DT, and QR-BRE algorithms, the dominant cost is TTM. For third-order tensors, the proposed QR-BRE algorithm consistently outperforms the other five algorithms in iteration speed across different ranks. The time proportion of TTM indicates that the branch reutilization of dimension tree provides superior acceleration compared to the dimension tree. The runtime ratio in the red line further confirms that the proposed QR-BRE algorithm consistently achieves shorter runtimes than the ALS algorithm. For fourth-order, fifth-order, and sixth-order tensors, the QR-BRE algorithm accelerates the QR algorithm regardless of rank. When the rank is small, it also outperforms the ALS algorithm

in iteration speed, as reflected in the red runtime ratio in Figure 7. Its significant computational advantage over the dimension tree is evident from the TTM proportion in the QR-DT and QR-BRE algorithms.

4.3 Synthetic tensors

This subsection primarily investigates synthetic tensors with a consistent true rank while varying factor collinearity, tensor dimensions, and noise levels. Specifically, two different sizes of third-order and fourth-order tensors are generated, each with a true rank of \hat{R} , different levels of factor collinearity, and varying noise conditions. The collinearity in each mode is represented by c_i . Homoscedastic noise is introduced with an intensity controlled by the parameter l_1 . When $l_2 > 0$, heteroscedastic noise is additionally introduced into the tensor, with l_2 controlling its proportion.

These tensors are generated following the procedures outlined in references [1, 10], and [39]. The main steps are as follows: First, specify the true rank \hat{R} , tensor size, parameters l_1 and l_2 , and the collinearity coefficients c_i . Second, generate an $R \times R$ matrix \mathbf{K} , where the diagonal elements are all 1, and the off-diagonal elements are the collinearity coefficient c_i . Third, compute the Cholesky factor \mathbf{C} of the \mathbf{K} . Fourth, create a matrix \mathbf{M} of size $I \times R$ with elements sampled from a standard normal distribution, and perform column-wise orthogonal normalization to obtain \mathbf{Q} . Finally, generate the n th factor matrix $\hat{\mathbf{B}}^{(n)} = \mathbf{Q}\mathbf{C}$. This process generates multiple factor matrices $\hat{\mathbf{B}}^{(n)}$, which are then used to construct the tensor \mathcal{X} . For $0 \leq l_1 < 100$, homoscedastic noise is added to the tensor \mathcal{X} as follows.

$$\mathcal{X}' = \mathcal{X} + \frac{1}{\sqrt{100/l_1 - 1}} \frac{\|\mathcal{X}\|_F}{\|\mathcal{N}_1\|_F} \mathcal{N}_1.$$

The size of tensor \mathcal{N}_1 matches that of tensor \mathcal{X} , and the elements of tensor \mathcal{N}_1 are drawn from a standard normal distribution. When $l_1 = 0$, $\mathcal{X}' = \mathcal{X}$, and when l_1 is close to 100, \mathcal{X}' approximates random noise. When $0 \leq l_2 < 100$ and $l_2 > 0$, heteroscedastic noise is added to the tensor \mathcal{X}' as follows.

$$\mathcal{X}'' = \mathcal{X}' + \frac{1}{\sqrt{100/l_2 - 1}} \frac{\|\mathcal{X}'\|_F}{\|\mathcal{N}_2\|_F} \mathcal{N}_2,$$

where the elements of tensor \mathcal{N}_2 are drawn from a normal distribution with mean 0 and standard deviation 3. When $l_2 = 0$, $\mathcal{X}'' = \mathcal{X}'$ and l_2 is approaches 100, \mathcal{X}'' is approximates random noise. The detailed parameters of the synthetic tensors used in the experiment can be found in Table 8.

Table 8: The detailed parameters of the synthetic tensor.

third-order	tensor size	c_1, c_2, c_3	\hat{R}	R	l_1	l_2
1	[500 500 500]	[0.9 0.9 0.9]	20	10	0.01	0
2	[500 500 500]	[0.9 0.9 0.9]	20	20	0.01	0
3	[500 500 500]	[0.9 0.9 0.9]	20	30	0.01	0
4	[600 600 600]	[0.5 .09 .09]	20	10	0.01	0.1
5	[600 600 600]	[0.5 .09 .09]	20	20	0.01	0.1
6	[600 600 600]	[0.5 .09 .09]	20	30	0.01	0.1
fourth-order	tensor size	c_1, c_2, c_3, c_4	\hat{R}	R	l_1	l_2
7	[100 100 100 100]	[0.9 0.9 0.9 0.9]	20	10	0.1	0
8	[100 100 100 100]	[0.9 0.9 0.9 0.9]	20	20	0.1	0
9	[100 100 100 100]	[0.9 0.9 0.9 0.9]	20	30	0.1	0
10	[120 120 120 120]	[0.5 0.9 0.9 0.5]	20	10	0.1	0.01
11	[120 120 120 120]	[0.5 0.9 0.9 0.5]	20	20	0.1	0.01
12	[120 120 120 120]	[0.5 0.9 0.9 0.5]	20	30	0.1	0.01

In all experiments involving synthetic and real-world tensors, the two extrapolation hyperparameters for Algorithm 3 are selected according to the following rules: The hyperparameter α is fixed at $\frac{1}{10}$. The hyperparameter β is chosen only if the difference in fitting performance between the first

two iterations is less than 0.03. If the fitting coefficient at this point exceeds 0.90, β is set to $\frac{1}{2000}$; if the fitting coefficient is between 0.70 and 0.90, β is set to $\frac{1}{500}$; otherwise, β is set to $\frac{1}{250}$. Once β is selected, its value remains fixed throughout subsequent iterations.

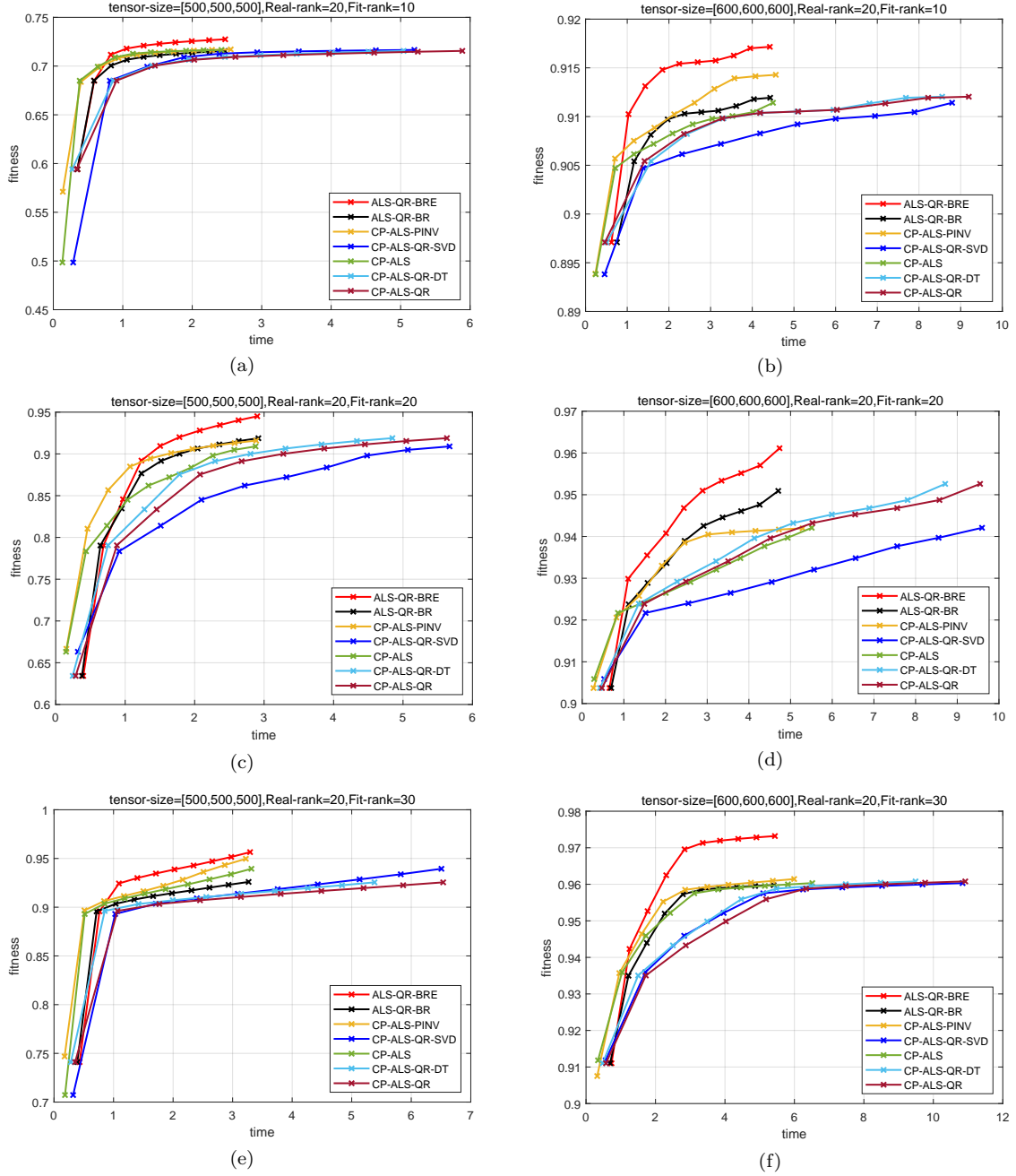


Figure 8: The performance plots of the third-order tensor after 20 iterations. The left panel displays the performance for different fitting ranks and a single type of noise on the tensor of size $[500, 500, 500]$. The right panel shows the performance for different collinearity coefficients, different fitting ranks and mixed noise types on the tensor of size $[600, 600, 600]$.

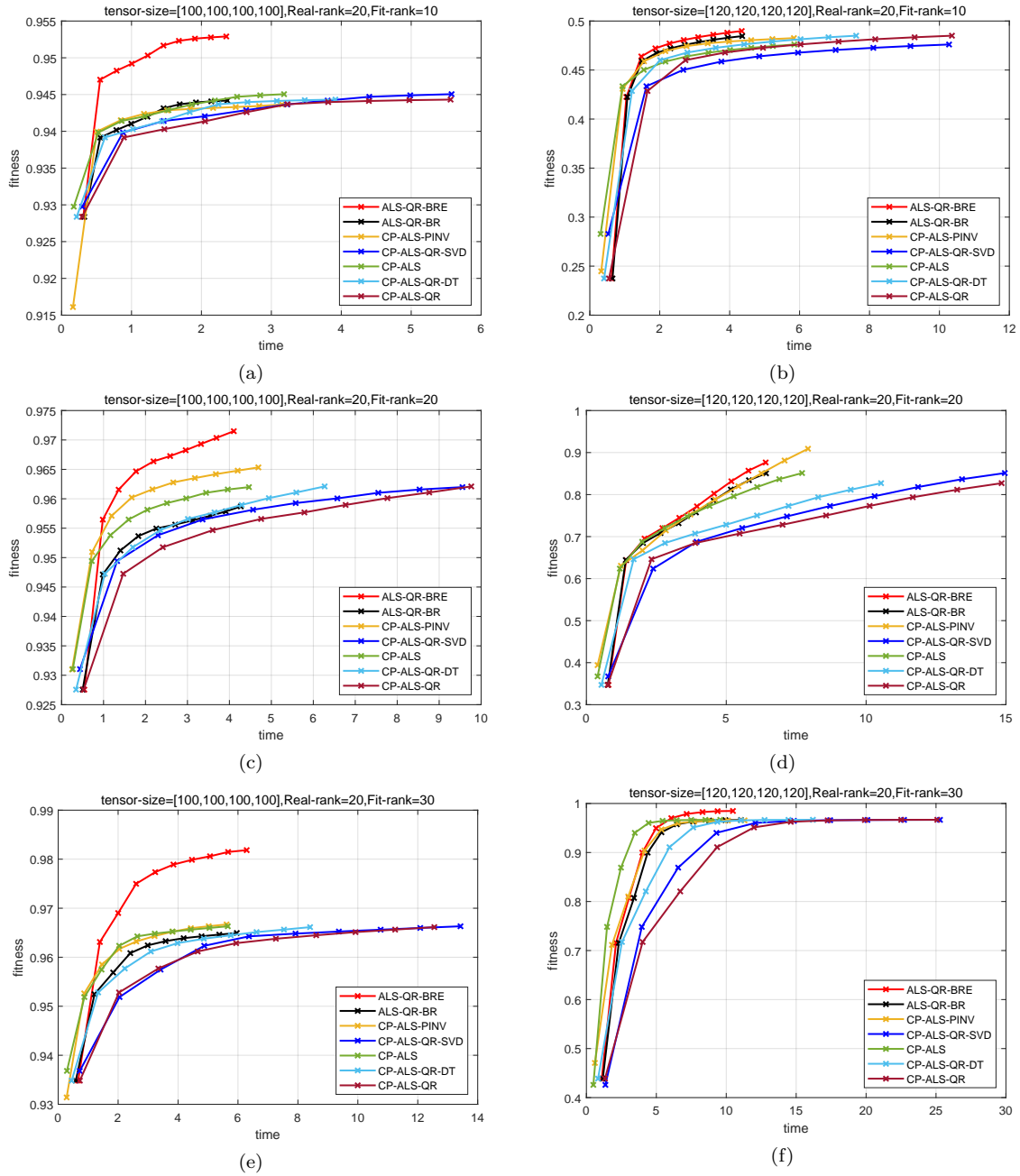


Figure 9: The performance plots of the fourth-order tensor after 20 iterations. The left panel displays the performance for different fitting ranks and a single type of noise on a tensor of size $[100, 100, 100, 100]$. The right panel shows the performance for different collinearity coefficients, different fitting ranks, and mixed noise types on a tensor of size $[120, 120, 120, 120]$.

We present the experimental results of ALS-QR-BRE, ALS-QR-BR, CP-ALS, CP-ALS-PINV, CP-ALS-QR-SVD, CP-ALS-QR-DT, and CP-ALS-QR algorithms on synthetic third-order and fourth-order tensors (the details of synthetic tensors shown in Table 8) in Figures 8 and 9. The experiments involve running each algorithm for 20 iterations, after which we compare the time required for 20

iterations and the fitting accuracy. From Figure 8, we conclude that our proposed ALS-QR-BRE and ALS-QR-BR algorithms require approximately half the iteration time of the CP-ALS-QR and CP-ALS-QR-SVD algorithms across different fitting ranks. Although the CP-ALS-QR-DT algorithm accelerates the CP-ALS-QR algorithm, the improvement is minimal, and our proposed algorithms remain faster than CP-ALS-QR-DT. In most cases, our proposed algorithms exhibit comparable or slightly faster iteration speeds than CP-ALS and CP-ALS-PINV, as shown in Figures 8(d) and 8(f). Moreover, the ALS-QR-BRE algorithm consistently achieves superior fitting accuracy compared to the other algorithms across all synthesized third-order tensors and fitting ranks. From Figure 9, we find that our proposed ALS-QR-BRE and ALS-QR-BR algorithms require less than half the iteration time of CP-ALS-QR and CP-ALS-QR-SVD across different fitting ranks. While the CP-ALS-QR-DT algorithm accelerates CP-ALS-QR and CP-ALS-QR-SVD, it still lags behind our proposed algorithms. For the majority of cases, our proposed algorithms match or surpass CP-ALS and CP-ALS-PINV in iteration speed, except for a slight delay in Figure 9(e). In particular, the ALS-QR-BRE algorithm consistently achieves a higher approximation accuracy across all synthesized fourth-order tensors and fitting ranks, with particularly significant improvements in Figures 9(a), 9(c), and 9(e).

The synthetic tensor experiments (Figures 8 and 9) demonstrate that the proposed ALS-QR-BRE algorithm significantly reduces the iteration time of CP-ALS-QR and outperforms CP-ALS-QR-DT in computational efficiency. Its iteration speed is generally comparable to or faster than CP-ALS, while delivering better fitting accuracy than other algorithms.

4.4 Real-world datasets

In this subsection, we evaluate our algorithm on five real-world datasets: *Indian Pines*, *Salines*, *Density*, *Tabby Cat*, and *Winter Landscape*.

- *Indian Pines*¹: The dataset is hyperspectral data collected by the AVIRIS sensor from the Indian Pines test site in northwestern Indiana. The data contains 145×145 pixels and 224 spectral bands, primarily covering agricultural land and natural vegetation such as forests.
- *Salines*: This dataset is a hyperspectral remote sensing image also collected by the AVIRIS over the Salinas Valley region in California, USA. The dataset contains 224 contiguous spectral bands with high spatial resolution. The spatial dimensions span 512 rows and 217 columns, forming a third-order tensor with dimensions $512 \times 217 \times 224$.
- *Density*²: This dataset is a third-order tensor representing the dynamic interaction between two fluids with different densities in a simulation. It has a 3D grid of size $2048 \times 256 \times 256$ (Z, Y, X), stored in double precision format (1 GB), providing detailed insights into fluid dynamics.
- *Tabby Cat*³: This dataset is derived from a standard color video source, where the initial temporal segment of the footage has been processed to form a fourth-order tensor with dimensions $720 \times 1280 \times 3 \times 48$.
- *Winter Landscape*⁴: This dataset also is derived from a standard color video source, where the initial temporal segment of the footage has been processed to construct a fourth-order tensor with dimensions $1510 \times 1080 \times 3 \times 60$.

For each real-world tensor experiment, we run the ALS-QR-BRE, ALS-QR-BR, CP-ALS, CP-ALS-PINV, CP-ALS-QR-SVD, CP-ALS-QR-DT, and CP-ALS-QR algorithms for 20 iterations to evaluate and compare their iteration efficiency and fitting accuracy. The experimental results are presented in Figures 10–13. Since the computational overhead introduced by extrapolation is negligible, the

¹https://www.ehu.es/ccwintco/index.php/Hyperspectral_Remote_Sensing_Scenes

²https://gitlab.com/tensors/tensor_data_miranda_sim

³<https://www.pexels.com/video/video-of-a-tabby-cat-854982/>

⁴<https://www.pexels.com/video/an-animal-on-a-winter-landscape-2313069/>

time advantage of the ALS-QR-BRE iterations is essentially the same as that of the ALS-QR-BR algorithm.

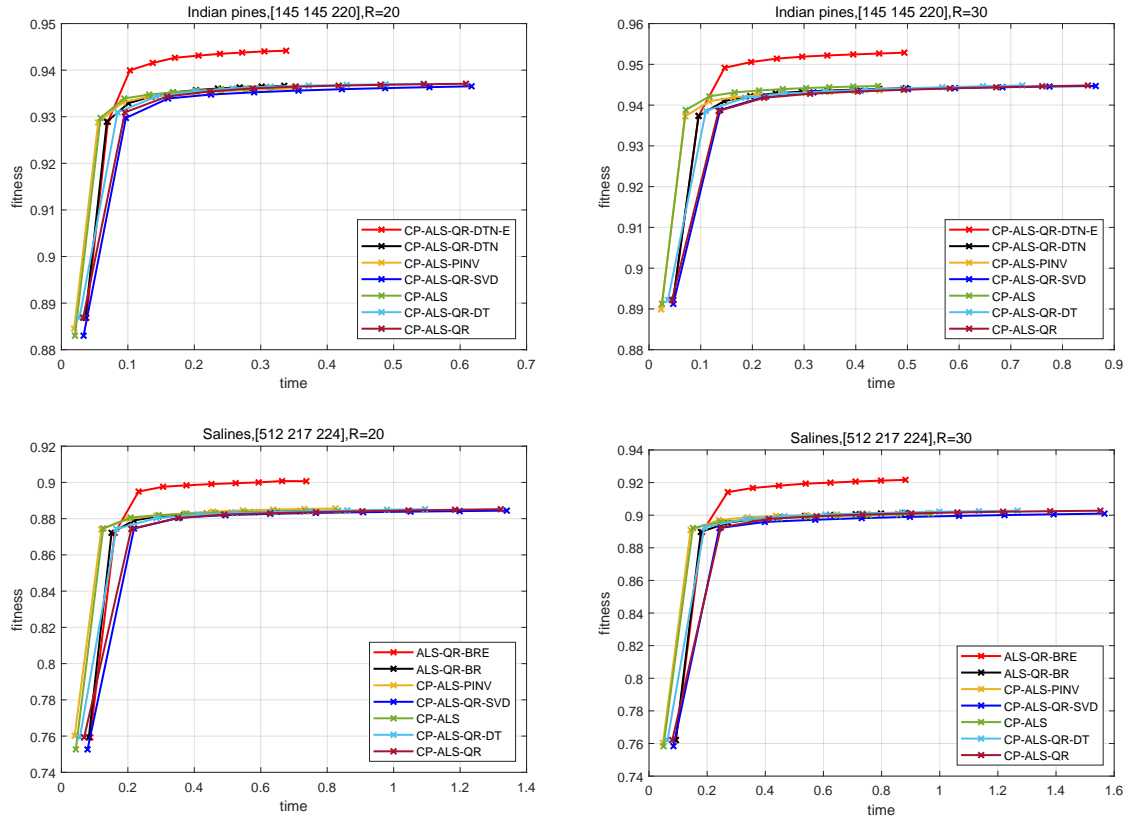


Figure 10: The performance plots of each algorithm over iterations on the Indian Pines and Salines datasets are presented. The left panel displays the performance curve with a fitting rank of 20, while the right panel shows the performance curve with a fitting rank of 30.

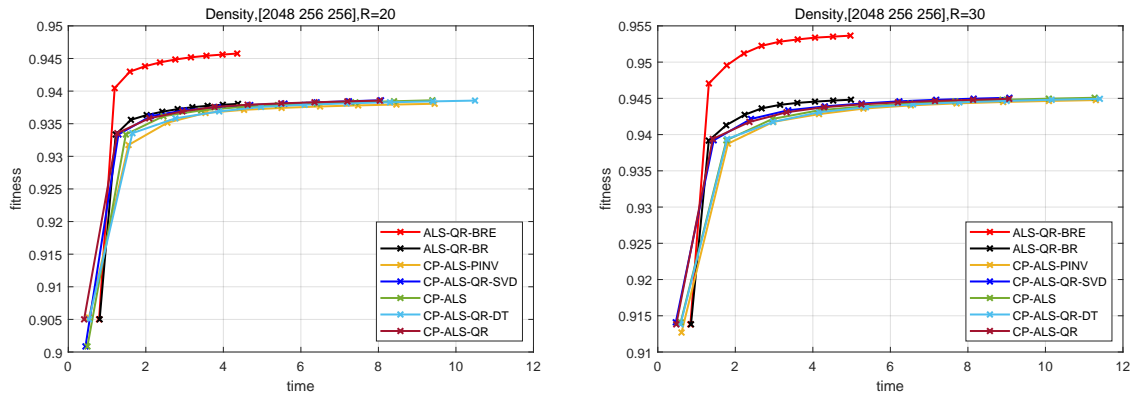


Figure 11: Performance plots of each algorithm over iterations on the Density dataset are shown. The left panel displays the performance plot with a fitting rank of 20, while the right panel shows the performance plot with a fitting rank of 30.

We present the rank-20 and rank-30 decompositions of the third-order tensor datasets *Indian*

Pines and *Salines* in Figure 10. It shows that for the rank-20 decomposition on the *Indian Pines* dataset, our proposed algorithm ALS-QR-BRE achieves a faster iteration speed while enhancing fitting accuracy by 0.80% compared to its counterparts. For the rank-30 decomposition, it maintains a computational advantage over all algorithms except CP-ALS and CP-ALS-PINV, with a 0.86% improvement in fitting accuracy. In the data set *Salines*, regardless of whether the rank is 20 or 30, our proposed algorithm not only completes 20 iterations in a shorter time, but also achieves a superior fit accuracy, outperforming other algorithms by approximately 2%, while other algorithms converge to the same fit threshold.

We perform rank-20 and rank-30 decompositions for the *Density* dataset, and the results are shown in Figure 11. The results show that for rank-20 decomposition, our proposed algorithm ALS-QR-BRE completes the iterations in 53.5% of the time required by CP-ALS-QR and CP-ALS-QR-SVD, and in 45% of the time needed by CP-ALS and CP-ALS-PINV, while achieving a 0.75% improvement in fitting accuracy. For rank-30 decomposition, the ALS-QR-BRE method shows a similar advantage in iteration time and a 0.90% improvement in fitting accuracy.

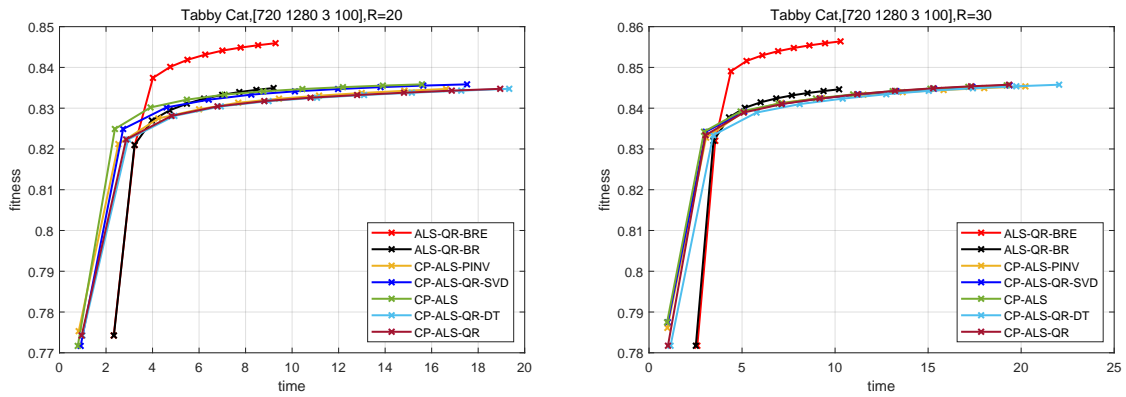


Figure 12: Performance plots for each algorithm over iterations on the Tabby Cat dataset. The left and right panels display the performance plots for different algorithms with ranks of 20 and 30, respectively.

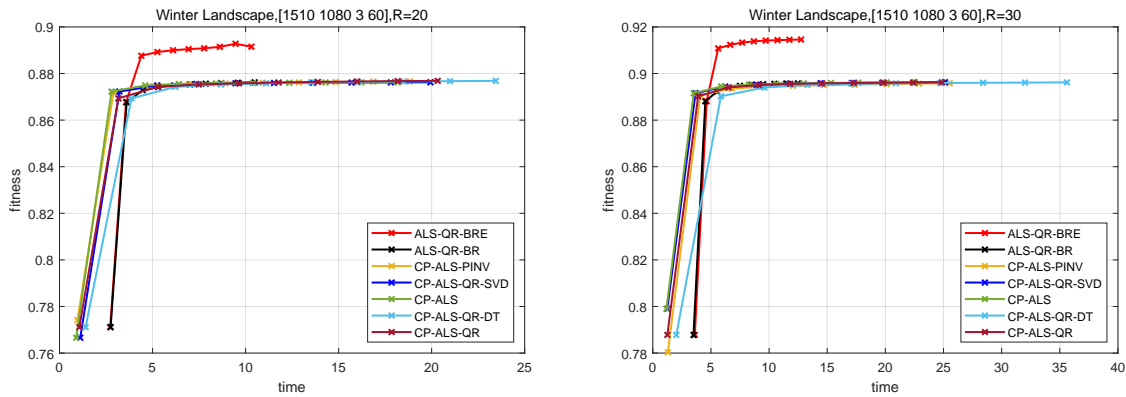


Figure 13: Performance plots for each algorithm over iterations on the Winter Landscape dataset. The left and right panels display the performance plots for different algorithms with ranks of 20 and 30, respectively.

Finally, in the experiment on real-world datasets, we use two fourth-order tensor datasets, *Tabby Cat* and *Winter Landscape*, to demonstrate the performance of our algorithm on large-scale tensors.

Similarly, we perform rank-20 and rank-30 decompositions for both datasets, and the results are presented in Figures 12 and 13. From Figure 12, we observe that for rank-20 decomposition, our proposed algorithm ALS-QR-BRE improves fitting precision by at least 1.26% compared to other algorithms, completing iterations in 48.1% of the time of the CP-ALS-QR algorithm and 57.7% of the time of the CP-ALS algorithm. For rank-30 decomposition, it finishes in 51.6% of the time of the CP-ALS-QR algorithm and 51.8% of the time of the CP-ALS algorithm, while improving fitting precision by 1.27%. Figure 13 shows that for rank-20 decomposition, the proposed ALS-QR-BRE algorithm improves the fitting accuracy by 1.74% compared to other algorithms, with the iteration time being 49.9% and 55.7% of those of the CP-ALS-QR and CP-ALS algorithms, respectively. For rank-30 decomposition, the iteration times are 49.7% and 54.4%, while the fitting accuracy improves by 2.07% compared to other algorithms.

Experimental evaluations on both synthetic and real-world tensor datasets demonstrate that the proposed ALS-QR-BRE algorithm consistently achieves shorter iteration times than the CP-ALS-QR algorithm. On real-world tensor datasets, it also exhibits faster convergence than CP-ALS. Furthermore, whether applied to synthetic or real-world tensors, the proposed ALS-QR-BRE algorithm consistently outperforms other compared algorithms in terms of fitting performance.

5 Conclusion

In this paper, we proposed branch reutilization of dimension tree, which effectively improved the utilization of intermediate tensors, thereby reducing the number of TTM operations and achieving a reduction in computational complexity. Additionally, we designed an extrapolation acceleration technique for the matrix \mathbf{Q}_0 in the CP-ALS-QR algorithm and provided an explanation of its design. By integrating branch reutilization of dimension tree and extrapolation techniques, we proposed the ALS-QR-BRE algorithm. Experiments conducted on both synthetic and real-world tensor datasets demonstrated that our proposed algorithm achieved improvements in both computational efficiency and fitting accuracy compared to other compared algorithms.

There are still several potential avenues for optimization in future work. When handling larger datasets and higher ranks, the computation of \mathbf{Q}_0 remains the primary computational bottleneck of the algorithm. Effectively leveraging the upper triangular structure of \mathbf{Q}_0 could further reduce runtime, especially for large-scale datasets. Additionally, further research is needed to optimize the selection mechanism of parameter β and to develop more efficient acceleration techniques.

Declarations

Funding: This research is supported by the National Natural Science Foundation of China (NSFC) grants 92473208, 12401415, the Key Program of National Natural Science of China 12331011, the 111 Project (No. D23017), the Natural Science Foundation of Hunan Province (No. 2025JJ60009).

Data Availability: Enquiries about data/code availability should be directed to the authors.

Competing interests: The authors have no competing interests to declare that are relevant to the content of this paper.

References

- [1] E. Acar, D. M. Dunlavy, and T. G. Kolda. A scalable optimization approach for fitting canonical tensor decompositions. *The Journal of Chemometrics*, 25(2):67–86, 2011.
- [2] C. M. Andersen and R. Bro. Practical aspects of parafac modeling of fluorescence excitation-emission data. *The Journal of Chemometrics*, 17(4):200–215, 2003.

- [3] A. M. S. Ang and N. Gillis. Accelerating nonnegative matrix factorization algorithms using extrapolation. *Neural Computation*, 31(2):417–439, 2019.
- [4] B. W. Bader, T. G. Kolda, and et al. Tensor toolbox for matlab, version 3.2.1, 2021. Available from: www.tensortoolbox.org.
- [5] R. Bro. Parafac. tutorial and applications. *Chemometrics and Intelligent Laboratory Systems*, 38(2):149–172, 1997.
- [6] A. Carlson, J. Betteridge, B. Kisiel, B. Settles, E. R. Hruschka, and T. M. Mitchell. Toward an architecture for never-ending language learning. In *Proceedings of the 24th AAAI Conference on Artificial Intelligence*, pages 1306–1313. AAAI Press, 2010.
- [7] J. D. Carroll and J.-J. Chang. Analysis of individual differences in multidimensional scaling via an n-way generalization of “eckart–young” decomposition. *Psychometrika*, 35(3):283–319, 1970.
- [8] Y. Chen, D. Han, and L. Qi. New als methods with extrapolating search directions and optimal step size for complex-valued tensor decompositions. *IEEE Transactions on Signal Processing*, 59(12):5888–5898, 2011.
- [9] P. Comon, X. Luciani, and A. D. Almeida. Tensor decompositions, alternating least squares and other tales. *Journal of Chemometrics*, 23(9):393–405, 2009.
- [10] E. David and Y. Nan. Blockwise acceleration of alternating least squares for canonical tensor decomposition. *Numerical Linear Algebra with Applications*, 30:e2516, 2023.
- [11] L. De Lathauwer and B. De Moor. From matrix to tensor: Multilinear algebra and signal processing. In *Proceedings of the 4th International Conference on Mathematics and Its Applications*, pages 1–16, 1998.
- [12] S. Eswar, K. Hayashi, G. Ballard, R. Kannan, M. A. Matheson, and H. Park. Planc: Parallel low-rank approximation with nonnegativity constraints. *ACM Transactions on Mathematical Software.*, 47(3):1–37, 2021.
- [13] J. Goulart, M. Boizard, R. Boyer, G. Favier, and P. Comon. Tensor cp decomposition with structured factor matrices: Algorithms and performance. *IEEE Journal of Selected Topics in Signal Processing*, 9(6):1064–1077, 2015.
- [14] L. Grasedyck. Hierarchical singular value decomposition of tensors. *SIAM Journal on Matrix Analysis and Applications*, 31(4):2029–2054, 2010.
- [15] R. Harshman. Foundations of the parafac procedure: Models and conditions for an “explanatory” multi-modal factor analysis. *UCLA Working Papers in Phonetics*, 16:1–80, 1970.
- [16] R. A. Harshman. *Foundations of the PARAFAC Procedure: Models and Conditions for an Explanatory Multimodal Factor Analysis*. PhD thesis, University of California at Los Angeles, Los Angeles, CA, USA, 1970.
- [17] F. L. Hitchcock. The expression of a tensor or a polyadic as a sum of products. *Studies in Applied Mathematics*, 6(1-4):164–189, 1927.
- [18] T. Ji, T. Huang, X. Zhao, T. Ma, and G. Liu. Tensor completion using total variation and low-rank matrix factorization. *Information Sciences*, 326(1):243–257, 2016.
- [19] T. G. Kolda and B. W. Bader. Tensor decompositions and applications. *SIAM Review*, 51(3):455–500, 2009.

- [20] V. Lebedev, Y. Ganin, M. Rakhuba, I. Oseledets, and V. Lempitsky. Speeding-up convolutional neural networks using fine-tuned cp-decomposition. In *Proceedings of the 3rd International Conference on Learning Representations*, 2015.
- [21] N. Li, S. Kindermann, and C. Navasca. Some convergence results on the regularized alternating least-squares method for tensor decomposition. *Linear Algebra and Its Applications*, 438(2):796–812, 2013.
- [22] A. P. Liavas, G. Kostoulas, G. Lourakis, K. Huang, and N. D. Sidiropoulos. Nesterov-based alternating optimization for nonnegative tensor factorization: Algorithm and parallel implementation. *IEEE Transactions on Signal Processing*, 66(4):944–953, 2017.
- [23] X. Liu and K. K. Parhi. Tensor decomposition for model reduction in neural networks: A review. *IEEE Circuits and Systems Magazine*, 23(2):8–28, 2023.
- [24] R. Minster, I. Viviano, X. Liu, and G. Ballard. Cp decomposition for tensors via alternating least squares with qr decomposition. *Numerical Linear Algebra with Applications*, 30(5):e2511, 2023.
- [25] D. Mitchell, N. Ye, and H. De Sterck. Nesterov acceleration of alternating least squares for canonical tensor decomposition: momentum step size selection and restart mechanisms. *Numerical Linear Algebra with Applications*, 27(4):e2297, 2020.
- [26] C. Navasca, L. D. Lathauwer, and S. Kindermann. Swamp reducing technique for tensor decomposition. In *2008 16th European Signal Processing Conference*, pages 1–5. IEEE, 2008.
- [27] Y. Nesterov. A method of solving a convex programming problem with convergence rate $o\left(\frac{1}{k^2}\right)$. *Soviet Mathematics Doklady*, 27:372–376, 1983.
- [28] D. Nion, K. N. Mokiios, N. D. Sidiropoulos, and A. Potamianos. Batch and adaptive parafac-based blind separation of convolutive speech mixtures. *IEEE Transactions on Audio, Speech, and Language Processing*, 18(6):1193–1207, 2010.
- [29] I. V. Oseledets. Tensor-train decomposition. *SIAM Journal on Scientific Computing*, 33(5):2295–2317, 2011.
- [30] A. H. Phan, P. Tichavsky, and A. Cichocki. Tensorbox: a matlab package for tensor decomposition, 2013. Available from: <https://github.com/phananhhuu/TensorBox>.
- [31] M. Rajih, P. Comon, and R. A. Harshman. Enhanced line search: A novel method to accelerate parafac. *SIAM Journal on Matrix Analysis and Applications*, 30(3):1148–1171, 2008.
- [32] S. Rendle and L. Schmidt-Thieme. Pairwise interaction tensor factorization for personalized tag recommendation. In *Proceedings of the 3rd ACM International Conference on Web Search and Data Mining*, pages 81–90. ACM, 2010.
- [33] A. A. Rontogiannis, E. Kofidis, and P. V. Giampouras. Block-term tensor decomposition: Model selection and computation. *IEEE Journal of Selected Topics in Signal Processing*, 15(3):464–475, 2021.
- [34] N. D. Sidiropoulos, L. De Lathauwer, X. Fu, K. Huang, E. E. Papalexakis, and C. Faloutsos. Tensor decomposition for signal processing and machine learning. *IEEE Transactions on Signal Processing*, 65(13):3551–3582, 2017.
- [35] S. Smith and G. Karypis. A medium-grained algorithm for distributed sparse tensor factorization. In *Proceedings of the IEEE 30th International Parallel and Distributed Processing Symposium*, pages 902–911. IEEE, 2016.

- [36] M. Sonka, V. Hlaváč, and R. Boyle. *Image Processing, Analysis, and Machine Vision*. Cengage Learning, Stamford, CT, 4th edition, 2014.
- [37] P. Symeonidis, A. Nanopoulos, and Y. Manolopoulos. Tag recommendations based on tensor dimensionality reduction. In *Proceedings of the 2008 ACM Conference on Recommender Systems*, pages 43–50. ACM, 2008.
- [38] G. Tomasi. *Practical and Computational Aspects in Chemometric Data Analysis*. PhD thesis, University of Copenhagen, Copenhagen, Denmark, 2006.
- [39] G. Tomasi and R. Bro. A comparison of algorithms for fitting the parafac model. *Computational Statistics and Data Analysis*, 50:1700–1734, 2006.
- [40] L. R. Tucker. Some mathematical notes on three-mode factor analysis. *Psychometrika*, 31:279–311, 1966.
- [41] M. A. O. Vasilescu and D. Terzopoulos. Multilinear analysis of image ensembles: TensorFaces. In *European Conference on Computer Vision (ECCV) 2002*, volume 2350 of *Lecture Notes in Computer Science*, pages 447–460. Springer, 2002.
- [42] N. Vervliet, O. Debals, L. Sorber, M. Van Barel, and L. De Lathauwer. TensorLab 3.0, 2016. Accessed from: <https://www.tensorlab.net>.
- [43] L. Yuan, C. Li, D. Mandic, J. Cao, and Q. Zhao. Tensor ring decomposition with rank minimization on latent space: An efficient approach for tensor completion. *Proceedings of the AAAI Conference on Artificial Intelligence*, 33(1):9151–9158, 2019.